Tailoring the yttrium content in Ni-Ce-Y/SBA-15 mesoporous silicas for CO2 methanation

Chao Sun, Katarzyna Świrk, Ye Wang, Katharina Sarah Scheidl, Dag Werner Breiby, Magnus Rønning, Changwei Hu, Patrick da Costa

Tailoring the yttrium content in Ni-Ce-Y/SBA-15 mesoporous silicas for CO_2 methanation

Chao Sun, Katarzyna Świrk, Ye Wang, Katharina Sarah Scheidl, Dag Werner Breiby, Magnus Rønning, Changwei Hu, Patrick Da Costa

PII: S0920-5861(21)00346-1

DOI: https://doi.org/10.1016/j.cattod.2021.07.031

Reference: CATTOD13457

To appear in: *Catalysis Today*

Received date: 28 March 2021
Revised date: 13 July 2021
Accepted date: 21 July 2021

Please cite this article as: Chao Sun, Katarzyna Świrk, Ye Wang, Katharina Sarah Scheidl, Dag Werner Breiby, Magnus Rønning, Changwei Hu and Patrick Da Costa, Tailoring the yttrium content in Ni-Ce-Y/SBA-15 mesoporous silicas for CO_2 methanation, *Catalysis Today,* (2021) doi:https://doi.org/10.1016/j.cattod.2021.07.031

Tailoring the yttrium content in Ni-Ce-Y/SBA-15 mesoporous silicas for CO_2 methanation

Chao Sun[a*], Katarzyna Świrk[b], Ye Wang[a,d], Katharina Sarah Scheidl[e], Dag Werner Breiby[e], Magnus Rønning[b], Changwei Hu[c,d], Patrick Da Costa[a*]

[a]Institut Jean Le Rond d'Alembert, Sorbonne Université, CNRS UMR 7190, 2 Place de la Gare de Ceinture, 78210 Saint-Cyr-l'Ecole, France

[b]Department of Chemical Engineering, Norwegian University of Science and Technology (NTNU), Sem Sælands vei 4, 7491 Trondheim, Norway

[c]Key Laboratory of Green Chemistry and Technology, Ministry of Education, College of Chemistry, Sichuan University, 610064 Chengdu, China

[d]College of Chemical Engineering, Sichuan University, 610065 Chengdu, China

[e]PoreLab, Department of Physics, Norwegian University of Science and Technology (NTNU), Høgskoleringen 5, 7491 Trondheim, Norway

Email address: chao.sun@dalembert.upmc.fr; patrick.da_costa@sorbonne-universite.fr;

Abstract: A series of nickel-cerium-promoted mesoporous silica (SBA-15) catalysts modified with different loadings of yttrium were synthesized by cetyl trimethyl ammonium bromide (CTAB)-assisted impregnation. The catalysts were tested in CO_2 methanation reaction and characterized by N_2 sorption, small-angle X-ray scattering (SAXS) and wide-angle X-ray diffraction (XRD), H_2 chemisorption, transmission electron microscopy (TEM), X-ray photoelectron spectroscopy (XPS), H_2 temperature-programmed reduction (H_2-TPR), CO_2 temperature-programmed desorption (CO_2-TPD), and thermogravimetric analysis coupled with mass spectrometry (TGA-MS). The best catalytic performance in CO_2 methanation was found for Y-modified NiCe/SBA-15 catalysts, as compared to the unpromoted sample. The modification with 10 wt.% of yttrium gave the highest CO_2 conversion of 61 % ± 2 % at 350 °C. We attribute this

increase to an improved dispersion of Ni, increased reducibility of Ni species, higher ratio of $Ce^{3+}/(Ce^{3+}+Ce^{4+})$, and increased moderate basicity found for 15Ni10Ce10Y/SBA-15. This paper shows that 10 wt.% of Y loading not only improves the catalytic activity in CO_2 methanation, but also gives stable performance. The tested 15Ni10Ce10Y/SBA-15 catalyst did not exhibit activity loss during 7 h of time-on-stream (TOS) experiment at 350 °C. Moreover, carbon deposits and sintered nickel particles could hardly be found in the used 15Ni10Ce10Y/SBA-15 catalyst.

Graphical abstract

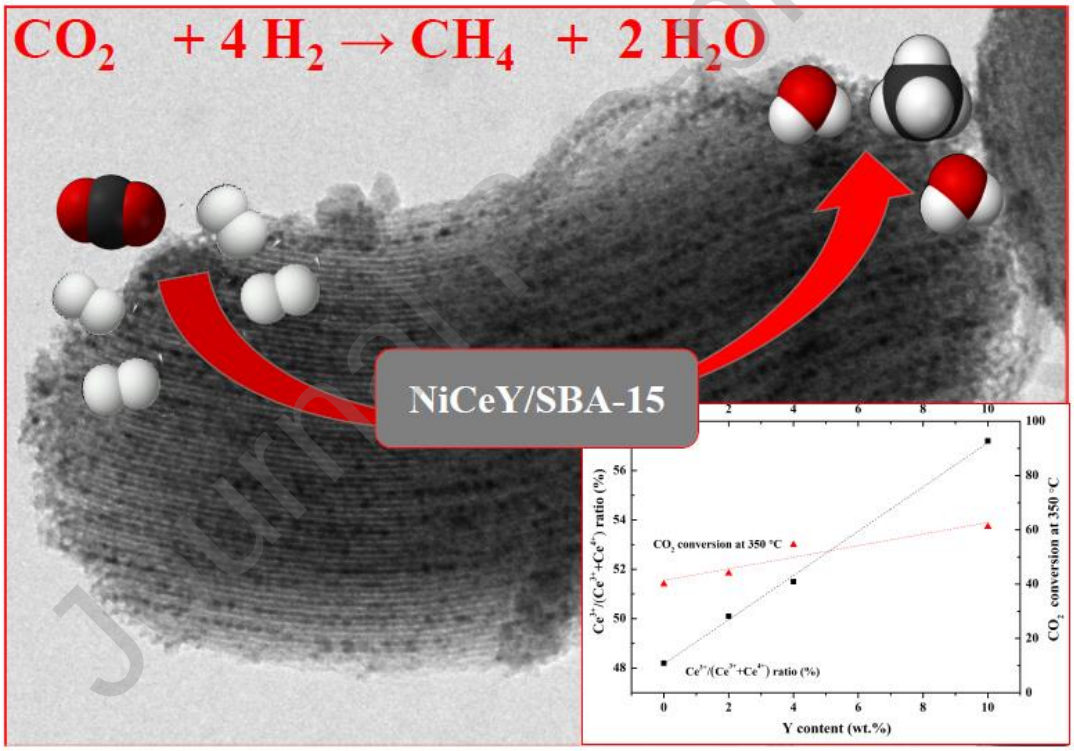

Keywords: CO_2 methanation, SBA-15, Nickel, Ce-Y promoters, Synergy

1. Introduction

The anthropogenic carbon dioxide (CO_2) from the combustion of fossil fuels has caused serious environmental problems since the rapid development of industrial society [1]. Increasing CO_2 concentration in the atmosphere leads to global warming, resulting in melting of glaciers, sea-level rise, species extinction, and frequent droughts/floods [1,2]. During the last decades, many efforts have been devoted to the reduction of CO_2 emissions [3–5]. CO_2 Capture and Storage (CCS) technology was developed to store excess CO_2 originating from power plants and industrial installations, but the relatively high cost of CCS equipment limits its broad application [4]. Moreover, the CCS approach mainly concentrates on the storage of CO_2, which is uneconomical. Meanwhile, CO_2 Capture and Utilization technology (CCU) has attracted much more attention worldwide due to its economic value. CCU can simultaneously reduce CO_2 emissions and produce valuable products. Catalytic conversion of CO_2 to chemicals and fuels plays a significant role in CCU technologies. Accordingly, carbon dioxide can be converted to syngas [6–8], methane [9–11], methanol [12], higher alcohols [13], diethyl ether [14] through a large variety of reactions. Hydrogenation of carbon dioxide, and CO_2 methanation in particular, has attracted attention of the academic community due to its numerous advantages. Meanwhile, the concept of Power to Gas (PtG) or Power to Methane (PtM) brings more possibilities to apply the CO_2 methanation reaction. In the PtM process, CO_2 can react with hydrogen (H_2) from electrolysis or photoelectrolysis of water using renewable energy sources, such as solar, wind, or hydropower. The produced methane represents the primary component in natural gas. Moreover, it can be easily incorporated into the natural gas pipelines for transportation. CO_2 methanation (1), also called Sabatier

reaction [15], is an exothermic and thermodynamically favorable reaction at low temperature:

$$CO_2 + 4H_2 = CH_4 + 2H_2O \qquad \Delta H_{298k} = -165 \text{ kJ/mol} \qquad (1)$$

Compared to other CO_2 hydrogenation reactions, CO_2 methanation has a greater potential to be used due to its high activity and selectivity, as well as the moderate conditions needed for the reaction. Nevertheless, CO_2 methanation still needs the participation of appropriate catalytic materials due to the existence of a kinetic barrier. Transition metal-based catalytic systems, such as Ni [9,16], Co [17], Pd [18], and Rh [19] based catalysts were found promising in the reaction. Among these catalytically active materials, Ni-based catalysts have attracted the most attention due to their numerous advantages, such as high availability, low cost, and high activity and selectivity [20].

Despite the beneficial aspects of Ni-based catalysts, there are still some problems that limit their industrial application. It has been reported that nickel-based catalysts are active mainly at temperatures higher than 300 °C [16,21,22]. Meanwhile, the CO_2 methanation is a highly exothermic reaction, thus the potential for sintering of Ni particles is relatively high [23]. Special attention should therefore be given to promoters and supports which can enhance the interaction and/or dispersion of nickel nanoparticles. A variety of materials, such as CeO_2 [24], ZrO_2 [25], Al_2O_3 [22,26], hydrotalcite [9,27], SiO_2 [28], SBA-15 [29–32], MCM-41 [30,33,34], KIT-6 [35], and SBA-16 [11,36], have been used as supports for preparation of Ni catalysts. Among mesoporous silicas, Santa Barbara Amorphous-15 (SBA-15) has attracted significant attention due to high specific surface area (up to 1160 m^2/g), particular pore size distribution (5-30 nm), large pore volume (up to 2.5 cm^3/g), well-ordered pore structure, and high thermal stability [37,38].

The highly ordered structure can limit the sintering of Ni particles at high temperatures, whereas an enhanced specific surface area and high pore volume contribute to the high dispersion of Ni active sites. SBA-15 has been extensively used as support for the preparation of Ni/SBA-15 catalysts. Liu et al. [32] synthesized Ni/SBA-15 catalysts by one-pot hydrothermal method (Ni/SBA-15-op) and conventional impregnation method (Ni/SBA-15-Im), investigating their catalytic performance in CO_2 methanation. It was found that Ni/SBA-15-op catalyst was more active than Ni/SBA-15-Im due to higher surface area, larger pore volume, and enhanced dispersion of nickel particles in Ni/SBA-15-op. Furthermore, the addition of promoters to Ni catalysts can significantly contribute to an improvement in catalytic efficiency. Bian et al. [39] synthesized the Ni/SBA-15 and Ni/Ce/SBA-15 catalysts by the sequential impregnation method and the dried Ni/Ce/SBA-15 (nitrate nickel) samples were processed by Dielectric Barrier Discharge (DBD) plasma and calcination in air. It was found that the Ce addition to Ni/SBA-15 significantly improved the activity and selectivity of the catalyst, regardless of the calcination or DBD plasma process. After modification with ceria, the catalyst decomposed by plasma (Ni/Ce/SBA-15-P) performed the best activity, which was attributed to the high dispersion of Ni, better reducibility, and increased number of basic sites. Apart from the process of plasma decomposition, Ni/Ce/SBA-15 catalysts calcined in air or vacuum were also reported in CO_2 methanation [31]. The study illustrated that the catalyst obtained under vacuum thermal treatment (Ni-CeO_2/SBA-15-V) showed better activity and selectivity compared to those thermally treated in air (Ni-CeO_2/SBA-15-air). This was attributed to the smaller particle size of Ni and CeO_2, as well as highly dispersed Ni species, being in close vicinity to Ce.

Other promoters, such as Zr [40,41], $Ce_xZr_{1-x}O_2$ [42], Y [43], Mg [29,44] were also used to enhance performance of Ni/SBA-15 catalysts in various catalytic reactions. Ce and Zr were commonly applied to improve nickel-based catalysts due to their redox and oxygen storage abilities. In our previous study [11], we found that Ce can distinctly improve the activity and selectivity of Ni/SBA-16 catalyst in CO_2 methanation. The presence of Ce led to an increase of Ce^{3+} ratio, moderate basicity, and Ni reducibility of Ni/Ce/SBA-16 catalyst. We also investigated modification with Y on the catalytic performance of Ni/CeO_2 in CO_2 methanation [10]. We showed that the incorporation of Y could substantially promote the activity of Ni/CeO_2. This presence of Y resulted in smaller CeO_2 crystal size, increased BET surface area, enhanced Ni-Ce metal-support interaction, and the increased oxygen vacancies for Y-doped Ni/CeO_2 catalysts.

Doping with promoters like Ce-Zr or Ce-Y on mesoporous materials supported Ni catalysts has been studied on reactions such as CO methanation and dry reforming of methane [45,46]. It has been demonstrated that Ni catalysts doped with *two* promoters showed better activity. Meanwhile, Ni/SBA-15 catalysts have been employed to catalyze the CO_2 methanation [29,32,47]. However, most studies previous studies have focused on the Ni/SBA-15 catalyst modified by only one promoter in CO_2 methanation.

To the best of our knowledge, the studies regarding the influence of Y and Ce promotion on Ni/SBA-15 catalyst have not been reported in CO_2 methanation. Herein, catalysts with fixed content of Ce (10 wt.%) and different loadings of Y (2, 4, 10 wt.%) were synthesized by co-impregnation method and characterized by a wide range of techniques targeting both structure and catalytic performance. The aim of this study is to

investigate the influence of Y on NiCe/SBA-15 catalyst in CO_2 methanation and the synergistic effects of Y and Ce when both are present.

2. Experimental part

2.1. Catalyst preparation

SBA-15 was synthesized by hydrothermal synthesis method as described by Han et al. [48]. In brief, Pluronic P123 (PEG-PPG-PEG, with average molar weight of 5800 g/mol, BASF) was dissolved in distilled water and the pH value of the aqueous solution was adjusted by adding HCl (37%, Sigma-Aldrich). After mixing thoroughly (45 min), TEOS (Tetraethyl orthosilicate, 98%, Sigma-Aldrich) was added dropwise to the above-mentioned solution and then stirred magnetically at 40 °C for 24 h. The molar ratio of the reaction mixture was controlled as TEOS/P123/HCl/H_2O=1/0.0168/5.8/155. The resulting mixture was aged at 65 °C for 120 h. Then, the precipitate was filtered and washed with distilled water followed by drying in an oven at 110°C for 12 h. The obtained solids were calcined at 550 °C for 5 h in synthetic air flow (20 ml/min) with a heating rate of 1 °C/min.

NiCe/SBA-15 catalysts modified with Y were prepared by co-impregnation in the presence of the surfactant cetyltrimethylammonium bromide (CTAB), which is widely used as a surfactant in the preparation of Ni catalysts [49–51]. Adding CTAB in the impregnation process was done to promote the dispersion of Ni particles. The Y content (x) in the NiCexY/SBA-15 catalysts varied from 2 to 10 wt.%, whereas a fixed amount of Ni (15 wt.%) and Ce (10 wt.%) was adjusted. The CTAB/Ni molar ratio was controlled at 0.3. In detail, the aqueous solution containing $Ni(NO_3)_2 \cdot 6H_2O$ (>99%, Sigma-Aldrich),

$Ce(NO_3)_3 \cdot 6H_2O$ (>99%, Sigma-Aldrich), $Y(NO_3)_3 \cdot 6H_2O$ (>99%, Sigma-Aldrich), and CTAB (>99 %, Sigma-Aldrich) was stirred for 30 min. Subsequently, the SBA-15 powder was added into the prepared solution and the magnetic stirring was maintained for 12 h at ambient temperature. Then, the obtained slurry was evaporated in a rotary evaporator (60 °C, 110 r/min). Thereafter, the material was dried in an oven at 100 °C for 12 h and calcined at 550 °C under synthetic air flow for 5 h with a heating rate of 5 °C/min (20 ml/min). The as-prepared catalysts were labeled as 15Ni10Ce/SBA-15 and 15Ni10CexY/SBA-15 (x= 2, 4, 10).

2.2. Catalyst characterization

N_2 physisorption isotherms, specific surface area (SSA), mesopore volume (V_p), and pore size distribution were measured at -196°C on a TriStar 3000 Micromeritics. Prior to the measurements, the samples were degassed for 3 h at 300°C using a Micromeritics VacPrep 061 degas unit. The specific surface area and pore size distribution were calculated by the Brunauer-Emmett-Teller (BET) and Barrett-Joyner-Halenda (BJH) methods, respectively.

The X-ray fluorescence (XRF) experiments were carried out in a Rigaku Supermini200 apparatus equipped with a proportional counter detector (PC) to determine the elemental composition of the samples. The measurements were performed under vacuum at 36.5℃ with the flow of P-10 gas (mixture of 10% CH_4/Ar; Flow rate: 24.7 mL/min). The sample was diluted in boric acid with a ratio of 1:200 and then pelletized under pressure of 10 bar. The samples were protected with polypropylene film of 6 mm before test.

The crystal structures of the calcined, reduced, and spent samples were determined by X-ray diffraction (XRD) performed on a Panalytical Empyrean diffractometer equipped with a copper-based anode (Cu-Kα, λ=0.154 nm) operated at 40 mA and 45 kV. The average crystallite size of NiO and metallic Ni was estimated by the Scherrer equation,

$$d = \frac{0.9\lambda}{B\cos\theta} \quad (1)$$

where d represents the average crystalline size, 0.9 is the Scherrer parameter, λ is the wavelength of the X-ray radiation given above, B denotes the full width at half maximum of the peak (FWHM), and θ is the angular position of the peak.

Small angle X-ray scattering (SAXS) measurements were carried out using a custom-built in-house setup at the Department of Physics, NTNU. The instrument is based on a Genix X-ray micro source from Xenocs, operating with an acceleration voltage of 50 kV and a tube current of 1 mA. The source sports a collimating multilayer mirror giving monochromatized CuK_α radiation (λ= 0.154 nm). The setup has a collimation path with two scatterless slits (also from Xenocs). A Pilatus 1M detector (Dectris Ltd.) with 981×1043 pixels and 172 μm^2 pixel size collected the scattered radiation, using an exposure time of 300 s. Calibration of the detector was done using silver behenate. The powdered sample was placed in a 1 mm glass capillary. Calibration and analysis of the data were performed using the software DAWN [52] and SimDiffraction [53].

H_2 chemisorption was employed to determine Ni dispersion (Micromeritics, ASAP 2020). Before analysis, about 0.2 g of calcined sample was evacuated in helium at 40°C. The sample was subsequently reduced in situ at 550°C for 1.5 h in the flow of H_2

(30 ml/min). The temperature was cooled down to 40°C, followed by the volumetric H_2 chemisorption with pure hydrogen.

Transmission electron microscopy (TEM) and Energy Dispersive X-ray spectroscopy (EDS) were carried out with JEM-2010 and JEM-2100Plus (JEOL, Tokyo, Japan) transmission electron microscopes operating at 200 kV for the reduced catalysts. Before measurement, the reduced samples (reduction condition: 550 °C for 1 h in 5 % H_2/Ar) were dispersed in ethanol, following the suspension being added dropwise on a copper grid covering with carbon film, then the prepared materials were used for the microscopy measurement.

X-ray photoelectron spectroscopy (XPS) analyses were performed using an AXIS Ultra DLD (KRATOS) spectrometer. The radiation was provided by a monochromatic Al source (Al-Kα, λ = 0.834 nm, operated at 15 kV, 10 mA). Before the measurement, the sample was reduced under 5% H_2/Ar flow (v/v; 100 ml/min) at 550 °C for 1.5 h and then cooled down to ambient temperature under H_2 mixture flow. Subsequently, the sample was positioned in the sample chamber and spectra were collected at room temperature. The registered spectra were referenced to the C1s peak at 284.6 eV. The carbon comes from the contamination during the preparation of sample.

The reducibility of the calcined catalyst was analyzed by temperature-programmed reduction in H_2 (H_2-TPR) performed on a BELCAT-M (BEL Japan Inc.). The apparatus is equipped with a thermal conductivity detector (TCD). Before the reduction step, around 60 mg of sample was pretreated in pure He (50 ml/min) at 350 °C for 1 h to remove moisture. Then, the material was cooled to 50 °C before being subjected to a mixture of 5% H_2/Ar (50 ml/min) for 10 min. Finally, the sample was

heated from 50 °C to 900 °C with a ramp of 10 °C/min under a 5% H_2/Ar mixture (50 ml/min). The consumption of H_2 was determined by fitting and integrating the TPR profiles. Bulk copper oxide was used as a reference of H_2 uptake.

The basicity of the catalyst was measured through a CO_2-TPD technique performed in the same apparatus as H_2-TPR. Prior to the measurement, the sample (60 mg) was pretreated in a 5% H_2/Ar flow of 50 ml/min at 550 °C for 1.5 h. Afterward, the sample was cooled down to 50 °C in the presence of H_2/Ar, followed by the flow of He (50 ml/min for 15 min). Then, CO_2 adsorption was conducted by flowing a mixture of 10% CO_2/He (50 ml/min, 1 h). Subsequently, a flow of He was applied for 30 min to desorb the physically adsorbed probe molecules. Finally, the TPD program was carried out in a He gas flow (50 ml/min) in the temperature range of 50–900 °C (heating rate 10 °C/min).

Thermogravimetry analysis coupled with mass spectrometry (Netzsch STA 449C Jupiter, MS: Netzsch Aëolos QMS 403C) was performed to analyze a possible coke formation on the surface of spent catalyst. The sample was heated from 35 to 900°C with heating rate 5°C/min under an air flow of 55 ml/min. Mass spectrometry was used to analyze the products of thermal decomposition of spent catalyst (mass-to-charge ratio: m/z = 44 for CO_2 and m/z = 18 for H_2O).

2.3. Catalytic activity tests of the catalysts in CO_2 methanation

The catalytic performance in CO_2 methanation was conducted in a U-type tubular quartz reactor (inner diameter 8 mm) at atmospheric pressure heated by an electric furnace, with a K-type thermocouple placed close to the catalyst bed to monitor the

temperature. Prior to the catalytic test, a sample of 0.5 ml volume was reduced in a mixture of 5% H_2/Ar (v/v; 100 ml/min) from ambient temperature to 550 °C and kept for 1.5 h with a temperature heating rate of 10 °C/min. After the reduction, the temperature decreased to 200 °C and the reaction gas mixture (CO_2/H_2/Ar = 15/60/25, 100 ml/min) was fed into the reactor, assuming gas hourly space velocity (GHSV) of 12,000 h^{-1}. The gas mixtures after reaction were analyzed by a gas chromatograph (Agilent, 490 Varian) equipped with a TCD detector. The flow rates of the inlet and outlet of the reactor were monitored by mass flow controllers (5850TR, Brooks). The reaction temperature range was 200-450 °C in steps of 50 °C and the reaction was maintained for 30 minutes at each temperature to reach a steady state. The outlet products registered by GC included CH_4 and CO. The CO_2 conversion and CH_4 selectivity were calculated by the following equations (2) and (3):

$$X_{CO_2}(\%) = \frac{F_{CO2,in} - F_{CO2,out}}{F_{CO2,in}} \times 100\% \qquad (2)$$

$$S_{CH_4}(\%) = \frac{F_{CH4,out}}{F_{CH4,out} + F_{CO,out}} \times 100\% \qquad (3)$$

where X represents CO_2 conversion; S represents CH_4 selectivity; F is the molar flow rate of the gas with "in" representing the inlet and "out" representing the outlet; The molar flows were obtained from the volume flow rates and the compositions from GC.

The CO_2 reaction rate per mass (r_{CO2}) and CH_4 formation rate per mass (r_{CH4}) of catalyst were calculated by equation (4) and (5) [54]:

$$r_{CO2} = \frac{F_{CO2,in} \times X_{CO2}}{m_{cat}} \qquad (4)$$

$$r_{CH4} = r_{CO2} \times S_{CH_4} \qquad (5)$$

where mcat represents the weight of catalyst; $F_{CO2,in}$ is the molar rate of CO_2 in inlet; XCO_2 and SCH_4 are the CO_2 conversion and CH_4 selectivity, respectively.

2.4. Isothermal stability tests of CO_2 methanation reaction

CO_2 methanation stability tests were performed in the same experimental setup as the previously conducted tests in the temperature range of 200-450 °C. The sample with the volume of 0.5 ml was pretreated at 550 °C under a mixture of 5% H_2/Ar flow (100 ml /min) for 1.5 h in atmospheric pressure following cooling down to 350 °C for the stability test, with a GHSV of 12,000 h^{-1}. Then, the reaction was maintained at 350 °C for 7 h. The stability tests were conducted at 350 °C because at this temperature CO_2 conversion values were distinguishable for the studied catalysts. CO_2 conversion and CH_4 selectivity were calculated by eq. (1) and (2), respectively.

3. Results and discussion

3.1. Catalyst Characterization

3.1.1. Textural properties, structural parameters, metal distribution, and chemical surface composition of the studied catalysts

The textural properties of the calcined samples were measured by N_2 physisorption. N_2 isotherms and pore size distributions are presented in **Fig. 1**. As shown in **Fig.1a**, all samples with and without yttrium showed type IV isotherm with H1 hysteresis loop, clearly demonstrating the presence of mesopores [55]. The parallel adsorption and desorption curves also indicate highly ordered cylindrical channels present in the samples. This analysis shows that the ordered 2D pore structure was preserved after modification with promoters. With the increasing yttrium loading, the inflection step slightly shifted towards lower relative pressure (p/p_0), indicating a slight

reduction of ordered mesopores [29]. The specific surface area (SSA), pore volume (V_p), and average pore width (D_{ap}) are presented in **Table 1**. As shown in **Table 1**, the as-synthesized SBA-15 has a high SSA and V_p (973 m^2/g and 1.09 cm^3/g). In this study, SSA and V_p of the studied Ni/SBA-15 catalysts are similar to those described in other reports on Ni/SBA-15 catalysts [56,57]. Despite a significant decrease of SSA observed for the Ce-promoted samples, the obtained values are still high and comparable to those reported elsewhere [43,46,58]. The decrease can be attributed to a cluster formation or deposition of promoter clogging the porous channels of the support [46]. Moreover, the still high SSA values indicate that the surfactant CTAB, added in the preparation step, can be a suitable reagent used during the synthesis of Ni/SBA-15 catalysts. Furthermore, the presence of Y did not cause a significant change regarding to the textural properties [9,10]. As presented in **Table 1**, SSA and V_p slightly increased with the increase of Y content until 4 wt.%. As for the sample containing 10 wt.% of Y loading, SSA and V_p were nearly the same as those for NiCe/SBA-15 sample. **Fig.1b** depicts BJH pore size distribution measured for the studied catalysts. The pore size of all the samples was mainly in the range of 2-8 nm. Metal oxides (Ni, Ce, and Y) deposited onto the SBA-15 support resulted in a slight decrease of the average pore size for NiCe/SBA-15 and NiCeY/SBA-15 samples, which can be linked with deposition of metal oxides inside the mesopores, which was has also been reported for La-promoted Ni/SBA-15 catalyst [47].

The NL-DFT pore size distributions curves are displayed in **Fig.S1**. As shown in Fig.S1, the catalysts displayed narrow NL-DFT pore size distributions with the maxima of the differential pore volume centered at 7.9 nm (15Ni10Ce/SBA-15). Compared to parent SBA-15, the pore size of the catalysts has slightly increased, which means the loss of

porosity reflects only blockage of micropores. Thus, the catalyst mainly retains the initial mesoporous texture of the parent SBA-15. This can account for the agglomeration of Ni particles on the external surface of SBA-15 as shown in TEM [59].

The XRF test was carried out to measure the elemental composition of 15Ni10Ce/SBA-15 catalyst. As shown in **Table S1**, the Ni and Ce contents are in consistent with the theoretical values, indicating that there was no significant loss of Ce and Ni in the preparation process.

Since all the catalysts were prepared by the same impregnation process, it can be speculated that there is also not large loss of the metal contents for Y-promoted catalysts.

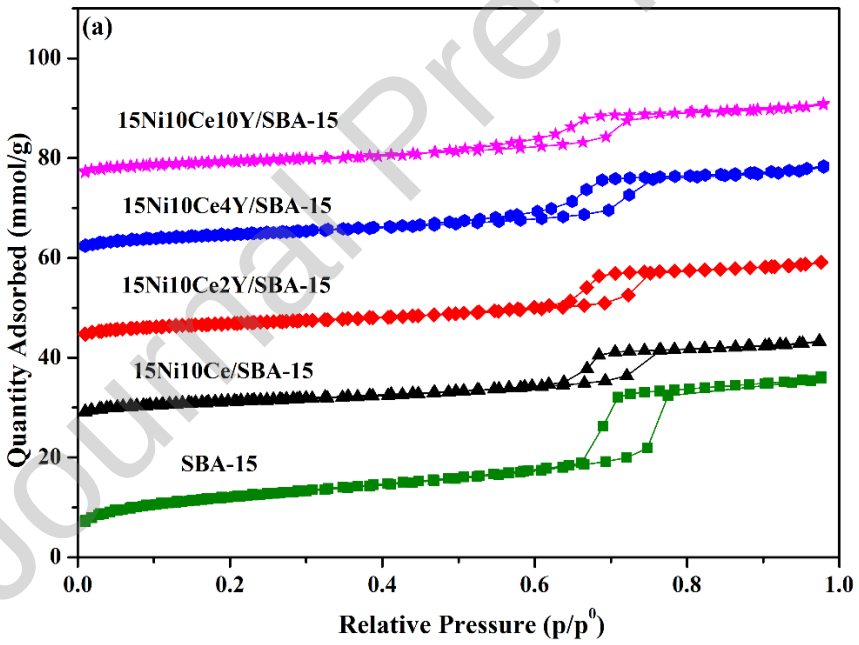

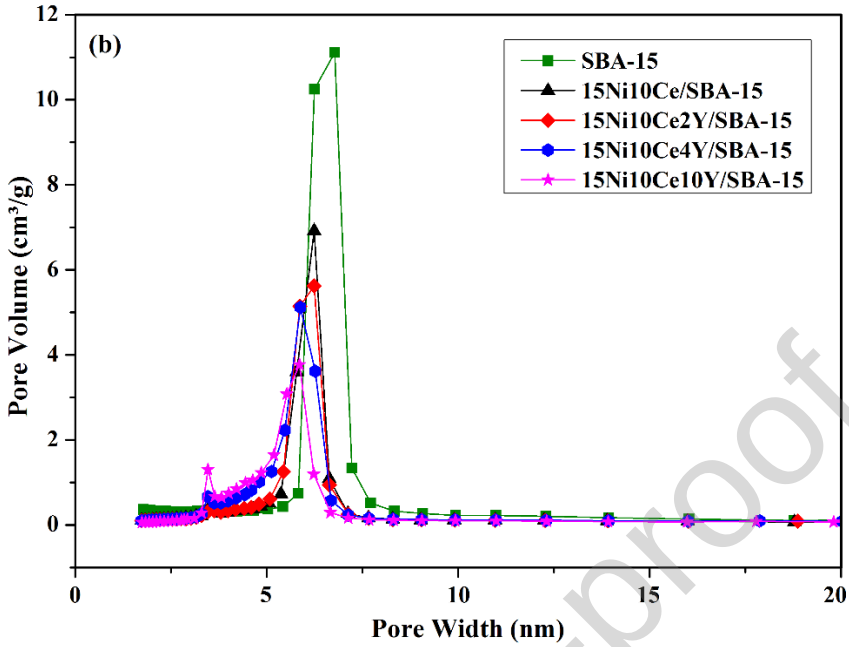

Figure. 1. N_2 adsorption-desorption isotherms a) and the BJH pore width distribution b) of the calcined catalysts. For clarity, the isotherms are vertically shifted.

The ordered structure of the calcined SBA-15, 15Ni10Ce/SBA-15, and 15Ni10Ce10Y/SBA-15 was studied by SAXS, presented as function of scattering vector $Q \equiv 4\pi\sin(\theta)/\lambda$, see **Fig. 2.** The Porod slope is markedly lower for the SBA-15 compared to the loaded samples, supporting a significant change in the catalyst morphology (including its specific surface area), from having rough surfaces towards being of more fractal nature. Three pronounced Bragg peaks, *100*, *110* and *200*, were observed for the samples investigated, with the most intense peak being at Q = 0.06 $Å^{-1}$. Their presence is attributed to the highly ordered 2D hexagonal structure (*p6mm*) which is the typical structure for SBA-15, having long cylindrical channels that are hexagonally packed [48,60]. These observations show that co-impregnation with Ni, Ce, and Y allows maintaining the ordered mesoporous structure of SBA-15 catalysts, however, their peaks

shifted towards higher 2θ angles (**Fig. 2**) as the unit cell parameter a decreased after modification with metals (**Table 1**). The measured hexagonal lattice values are in the range of a = 11.2-11.9 nm, being in good agreement with previous reports [60,61]. The recorded decrease in the unit cell parameter was due to a change of the thermodynamic properties governing the pore curvature etc. in the bulk of the catalyst particles. As presented in **Fig. 2**, the intensity of these small-angle diffraction peaks decreased after modifications with Ni-Ce and Ni-Ce-Y. This might be explained by several mechanisms, including either a partial destruction of the pore structure order of 15Ni10Ce/SBA-15 and 15Ni10Ce10Y/SBA-15 catalysts [47,62], or a reduced contrast between the pore and the matrix because of the partial filling of the pore.

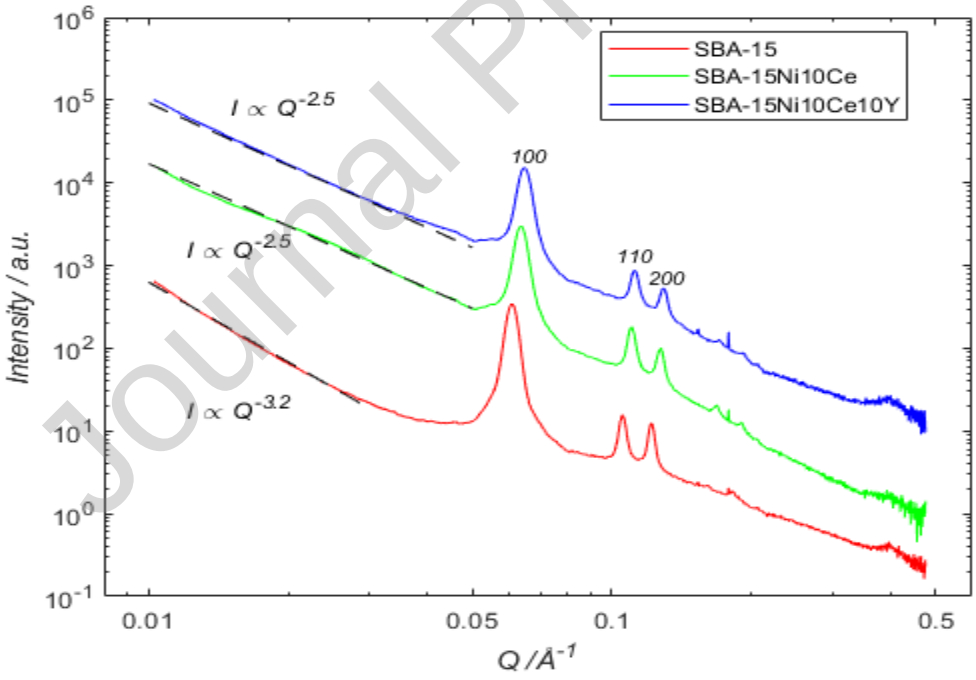

Figure. 2. SAXS patterns of the calcined SBA-15, 15Ni10Ce/SBA-15 and 15Ni10Ce10Y/SBA-15. Note the shift of the diffraction peaks with increasing loading. Also, the Porod exponent changes from about -3.2 ± 0.1 to -2.5 ± 0.1, signifying a change in the morphology of the catalyst particles.

The structural properties of the calcined and reduced catalysts were characterized by XRD and the recorded patterns are depicted in **Fig. 3**. As shown in **Fig. 3a**, the diffraction peaks at 2θ = 37.1, 43.1, 62.7, 75.2, and 79.3° were registered for all samples, which were assigned to the presence of (face centered cubic) NiO, and indexed as 111, 200, 220, 311, and 222, respectively [63,64]. For the calcined 15Ni10Ce/SBA-15 sample, only NiO was registered as a segregated phase. No separate phase of Ce species was observed which may indicate their high dispersion. By increasing the Y loading, two weak diffraction peaks located near 29°, at 28.9° and 33.1° appeared for the 15Ni10Ce10Y/SBA-15 sample, that may suggest existence of Y_2O_3 (ICSD reference no. 193377) and CeO_2 (ICSD reference no. 28753), respectively [10]. The modification with 10 wt.% Y loading may lead to a slight decrease of the dispersion of Y and Ce on the SBA-15 support due to the deposition of the metal species on the outer surface [65].

By increasing the Y loading, the diffraction peaks of CeO_2 and Y_2O_3 are still hard to identify, which means Ce and Y are highly dispersed on the support for Y-modified catalysts. Although there are no clear peaks of CeO_2 and Y_2O_3, a broad peak at 2θ of 28.94° on the 15Ni10Ce10Y/SBA-15 sample cannot be excluded, which may be assigned to the presence of Y.

Table 1. The textural properties, crystallite size of NiO and metallic Ni measured for the reduced samples.

Catalyst	SSA (m^2/g)[a]	V_p (cm^3/g)[b]	Crystallite size (nm)[c]		Crystallite size of Ni° (nm)[d]	Dispersion of Ni (%)[d]	Lattice Parameter *a* (nm)[e]
			NiO	Ni^0			
SBA-15	973	1.09	n/p	n/p	n/p	n/p	11.9
15Ni10Ce/SBA-15	400	0.54	13.4	19.5	11.0	3.2	11.4
15Ni10Ce2Y/SBA-15	410	0.55	14.0	21.5	12.1	3.1	n/m
15Ni10Ce4Y/SBA-15	443	0.61	15.3	17.1	12.5	3.1	n/m
15Ni10Ce10Y/SBA-15	395	0.53	15.3	21.0	11.4	3.4	11.2

n/p: not present. n/m: not measured
[a] Calculated by BET calculation method.
[b] Calculated by BJH desorption method.
[c] Calculated from XRD by the Scherrer equation.
[d] Calculated by H_2 chemisorption assuming spherical nickel crystallites of uniform size.
[e] Calculated from SAXS by $a=2d_{100}/\sqrt{3}$

Wide-angle XRD patterns of the reduced catalysts are depicted in **Fig. 3b**. The structural properties of the catalysts changed after reduction compared to the calcined samples. Only three peaks located at 2θ = 44.69, 52.03, and 76.60° were registered, which correspond to the *111*, *200* and *220* Bragg diffraction peaks of metallic Ni, respectively [36]. No peak was observed at around 2θ = 28.6° (expected location of CeO_2 and Y_2O_3) suggesting that the dispersion of Y or Ce was improved after reduction. Similarly to the calcined samples, a slight shift of the Bragg reflection from 2θ = 44.69° for 15Ni10Ce/SBA-15 to 2θ = 44.56° for 15Ni10Ce10Y/SBA-15 was found. Nevertheless, it is difficult to estimate whether an insertion of Ni atoms into the Ce or Si crystal structure occurred, as there was no clear diffraction peak of Ce, making the

comparison of cell parameter impossible [66]. However, the latter XPS characterization demonstrated that doping Y promoted the increase of $Ce^{3+}/(Ce^{3+}+ Ce^{4+})$ molar ratio.

Crystallite sizes of NiO and Ni° were estimated by the Scherrer equation (assuming no strain) and listed in **Table 1**. It can be seen that the crystallite sizes of metallic Ni were a litter larger compared to the NiO calculated for the calcined materials, which might be attributed the reduction step.

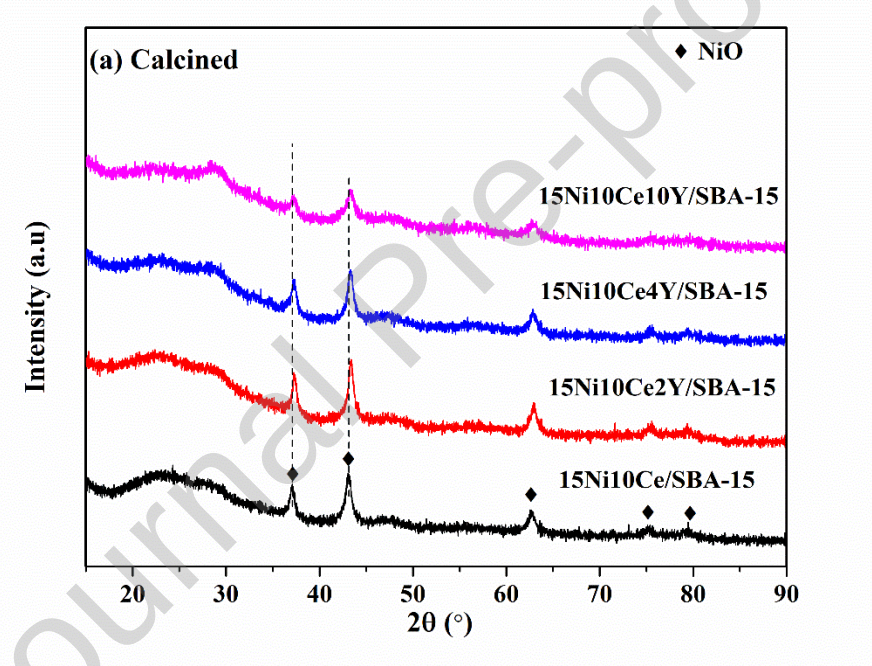

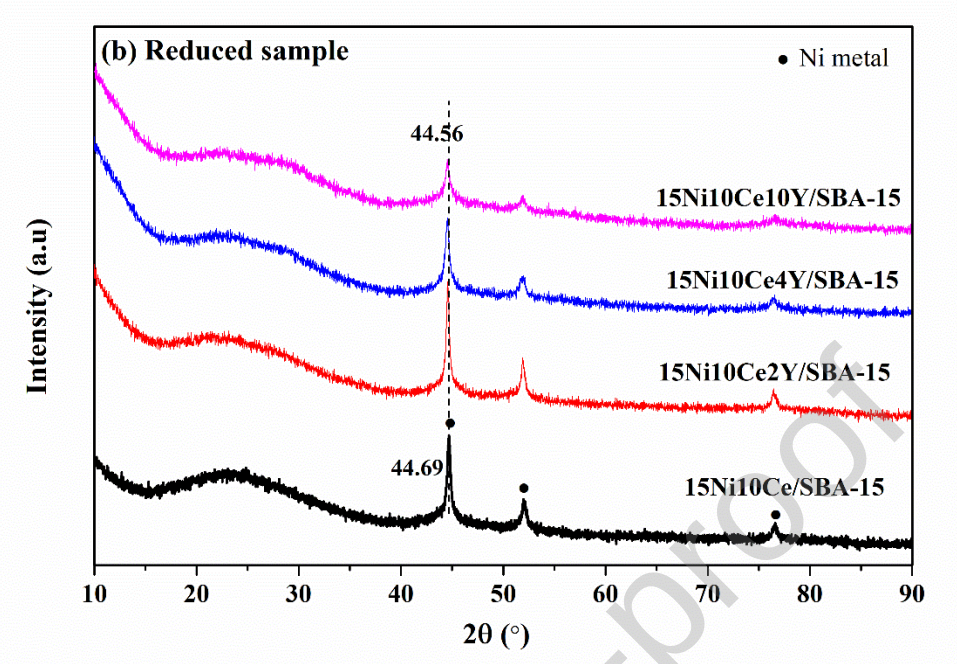

Figure 3. XRD patterns of the catalysts promoted with cerium and cerium-yttrium; (a) calcined samples, (b) reduced samples

H_2 chemisorption experiments were carried out and the dispersion of Ni, as well as the estimated size of Ni° crystallites, are presented in **Table 1**. With the increasing Y loading up to 4 wt.%, the dispersion of Ni did not change significantly. Furthermore, there is no significant difference regarding the Ni° particle size, indicating that the addition of Y has only a slight effect on active sites. The difference of Ni° particle size obtained from different methods (XRD or H_2 chemisorption) can be attributed to the effect of different measurements.

To directly image the mesoporous structure of SBA-15 and to determine the dispersion of Y_2O_3, CeO_2 and Ni° on the catalyst surface, EDS micrographs were obtained for the reduced catalysts. Micrographs are presented in **Fig.4** showing the presence of ordered arrays of long pores extending through the particles. These results

demonstrated that the distinct mesoporous-structure was maintained after impregnation with metals, fully consistent with the SAXS. **Fig.4a** shows micrographs of 15Ni10Ce/SBA-15 catalyst with large Ni particles (diameter up to 150 nm) that were probably formed by the agglomeration of nickel outside of the mesoporous channels of SBA-15. On the contrary, 15Ni10Ce10Y/SBA-15 catalyst presented well-dispersed Ni species inside the channels of the support (diameter less than 10 nm), with only a few larger Ni particles found on the outer surface of the catalyst (**Fig.4b**).

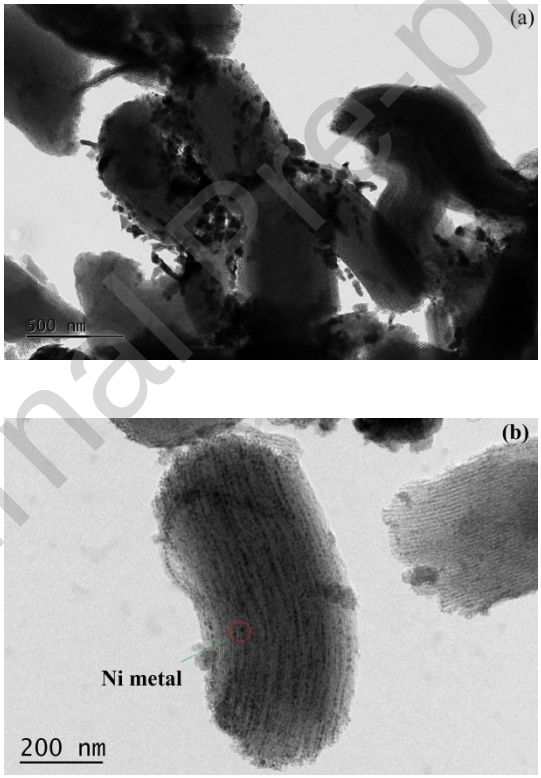

Figure. 4. TEM micrographs of the reduced catalysts; Conditions: 550 °C for 1.5h under 5%H_2/Ar; (a) 15Ni10Ce/SBA-15, (b) 15Ni10Ce10Y/SBA-15.

EDS elemental mapping analysis was carried out for 15Ni10Ce/SBA-15 and 15Ni10Ce10Y/SBA-15 and is presented in **Fig. S2a, and b**. In the former, Ce species were well dispersed over the support, whereas Ni was exposed in the form of big particles, as well as uniformly distributed nanoparticles. 15Ni10Ce10Y/SBA-15 revealed Y and Ce species evenly dispersed and less agglomerated particles of Ni. The reducibility of the studied catalysts will be described in detail in the next section.

In order to investigate the surface composition and oxidation states of the catalysts, XPS was performed for the reduced catalysts. The XPS spectra are shown in **Fig. S3** and the calculated atomic ratio and binding energies are given in **Table 2**.

As shown in **Fig. S3a**, the O1s spectrum can be deconvoluted into 3 peaks located at 530.4, 532.4, and 533.0 eV, which were attributed to the metal oxide (O_{OM}), oxygen of silica (O_{OSi}), and surface oxygen species adsorbed on oxygen defects (O_{OH}), respectively [67,68]. As shown in **Table 2**, doping Y resulted in the increase of O_{OH} species. Thus, it can be seen that the increment of Y loading lead to the increase of oxygen defects [69,70].

As shown in **Fig. S3b,** the overlapped spectra can be deconvoluted to 3 peaks. The intensive peak located at 154.0 eV was assigned to the presence of Si2s. The two weak peaks positioned at 157.5 and 159.8 eV were attributed to the presence of $Y3d_{5/2}$ and $Y3d_{3/2}$ [71]. As the Y loading increased, the peak intensity of Y_2O_3 increased, indicating that more yttria species deposited on the surface of the support. Also, no apparent peak shifts relating to $Y3d_{5/2}$ were registered (**Table 2**). From **Fig. S3c**, it can be seen that the intensity of Si2p peak, which is located at 103.1 eV, decreases with

increasingY loading, which can be attributed to the coverage of Ni, Ce, and Y on the surface of the SBA-15 material.

In **Fig.S3d**, the XPS spectra of $Ni2p_{3/2}$ for the for 15Ni10Ce/SBA-15 catalyst consisted of two peaks located at 852.8 and 855.5 eV, which were attributed to the Ni^0 and Ni^{2+} species ($Ni(OH)_2$) [72], with a shake-up satellite peak at 860.7 eV [73]. The presence of Ni^{2+} species was attributed to partial oxidization caused by exposure of the sample to air during the transportation for XPS. Also, the insufficient reduction of NiO cannot be excluded. In **Table 2**, the $Ni2p_{3/2}$ peak shifted towards higher binding energy as the increase of Y promotion, indicating the Ni species could also be incorporated into ceria lattice [70]. Meanwhile, higher Ni concentration on the surface of 10 wt.% Y-modified sample indicates high distribution of Ni on the surface [74].

The Ce3d XPS spectra of the catalysts are presented in **Fig.S3e**. With the increase of Y addition, the peak intensity of the Y-doped catalysts did not change much as compared with the peak intensity of Y-free catalysts. The Ce3d peak could be deconvoluted to 10 peaks labelled u^{iii}, u^{ii}, u^{i}, u, u^0, v^{iii}, v^{ii}, v^{i}, v, and v^0. The components labelled u^0, u^{i}, v^0, and v^{i} were attributed to Ce^{3+} species and the other components labelled u^{iii}, u^{ii}, u, v^{iii}, v^{ii}, and v were assigned to the presence of Ce^{4+} species [10]. From **Table 2**, it can be seen that the ratio of Ce^{3+}/Ce over the Y-doped catalysts increased gradually with the increase of Y loading, with the highest ratio of $Ce^{3+}/(Ce^{3+} + Ce^{4+})$ obtained over 10 wt.% Y promoted catalyst. Thus, it can be concluded that the dopant of Y promotes the formation of Ce^{3+}, and more oxygen vacancies are created, which are attributed to the intimate contact between Ce and Y, leading to replacement of Ce by Y [75]. As reported in literature [10,76,77], the Ce^{3+} (0.97 Å) can be substituted by Y^{3+}

(1.04 Å) in the lattice thanks to the similar ionic radii. The Ce3d peak position in energy for Y-doped catalysts also showed a slight shift with increasing Y loading towards lower binding energy, which demonstrates the incorporation of Y and Ni inside the Ce lattice over the catalysts. This is consistent with the results from XRD.

Table 2 XPS derived Ce^{3+} and Ni^0 percentage, Binding Energy of $Y3d_{5/2}$, $Ni2p_{3/2}$ and $Ce3d_{5/2}$ in eV, Ni, Ce, and Y atomic ratio for the samples after reduction.

Catalyst	Atomic ratio (%)					Binding Energy (eV)		
	Ni	Ce	Y	$O_{OH}/(O_{OM}+O_{OSi}+O_{OH})$	$Ce^{3+}/(Ce^{3+}+Ce^{4+})$	$Ni2p_{3/2}$	$Ce3d_{5/2}$	$Y3d_{5/2}$
15Ni10Ce/SBA-15	1.14	0.56	-	9.9	45.5	855.5	881.8	-
15Ni10Ce2Y/SBA-15	1.00	0.64	3.95	20.5	47.6	855.8	881.8	157.9
15Ni10Ce4Y/SBA-15	1.04	0.55	4.10	23.2	48.9	856.0	881.7	157.9
15Ni10Ce10Y/SBA-15	1.20	0.52	4.80	20.5	52.5	856.0	881.6	158.0

3.1.2. Reducibility of the studied catalysts

The reduction behavior was studied by H_2-TPR method and presented in **Fig.5**. Four peaks were revealed and labelled α, β, γ, and δ for 15Ni10Ce/SBA-15 and 15Ni10CexY/SBA-15 catalysts (**Figs. 5a-b**), and attributed to the reduction of Ni species with different degree of metal-support interactions [78,79]. The peaks centered at temperatures lower than 400 °C (α and β) were attributed to the reduction of NiO species located on the external surface of SBA-15 [79,80]. The peaks centered at 400-500 °C (γ) and 600 °C (δ) were assigned respectively to the reduction of NiO weakly and strongly interacting with the support [81]. **Fig.5** revealed a shift of the reduction peaks towards lower temperature with the increment of the Y content, except for the sample with 2 wt.%

of Y. This indicates that the reducibility of Y-promoted catalysts has been improved with the increasing loading of yttrium. **Table S2** presents the H_2 consumption calculated for Y-promoted NiCe/SBA-15 catalysts. The maximum of reduction peaks was lower except for those with 2 wt.% of Y-containing sample. The latter revealed maximum of reduction peaks similar to 15Ni10Ce/SBA-15 catalyst. TEM micrographs showed an agglomeration of Ni particles in the reduced 15Ni10Ce/SBA-15 sample, whereas the presence of Y facilitated the formation of small nickel particles. In this regard, the reducibility of NiO for15Ni10CexY/SBA-15 catalysts have been enhanced.

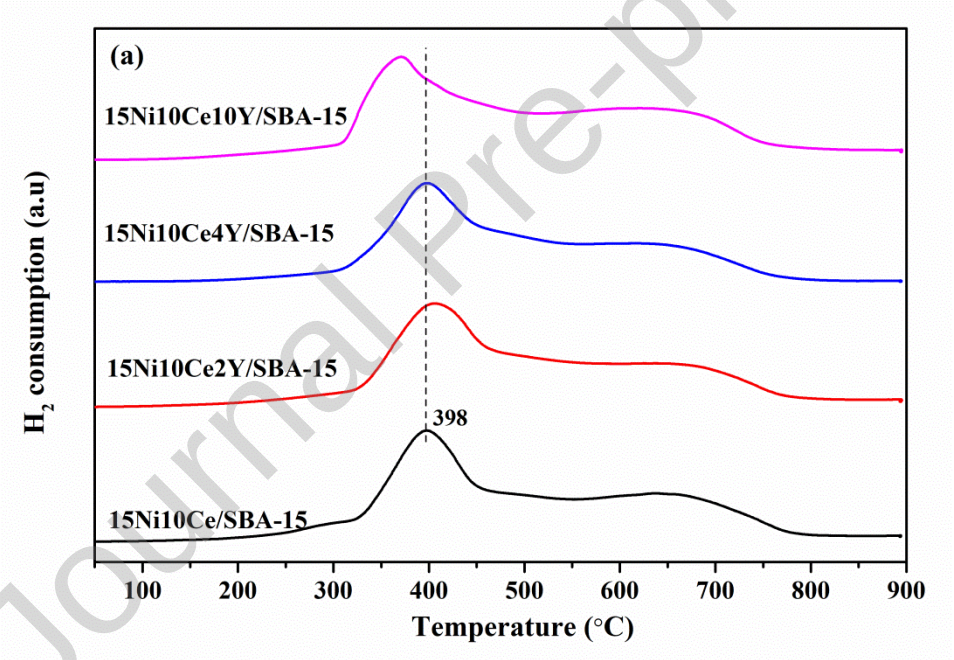

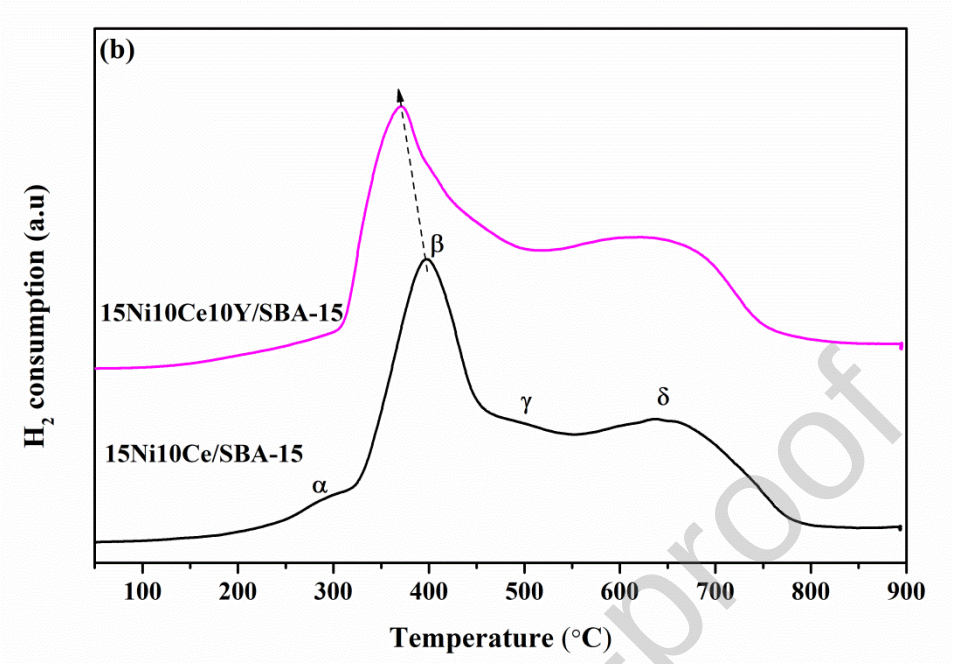

Figure. 5. H_2-TPR profiles of the as calcined catalysts (a) and the enlarged mapping of the profiles of 15Ni10Ce/SBA-15 and 15Ni10Ce10Y/SBA-15 (b)

3.1.3. Basicity of the studied catalysts

An adequate number of basic sites is known to play a crucial role in the catalytic performance of CO_2 methanation catalysts. Thus, the basicity of the studied catalysts was investigated by temperature-programmed desorption using CO_2 as a probe molecule. CO_2 desorption profiles are shown in **Fig.6** and the basic sites distribution listed in **Table 3**. The CO_2 desorption peaks can be classified to three types based on their temperature regions: <200 °C, 200-400 °C, and >400 °C corresponding to weak, medium, and strong basic sites, respectively [10,27,47]. As shown in **Table 3**, the medium basic sites and total number of basic sites increased with increasing Y loading. The highest amount of medium basic sites was obtained for 15Ni10Ce10Y/SBA-15 catalyst. Pan et al. [82] investigated the reaction route of CO_2 methanation over $Ni/Ce_{0.5}Zr_{0.5}O_2$ catalyst. The authors suggested that medium basic sites can promote the formation of monodentate

carbonates, enhancing activity in CO_2 methanation. Similar observations regarding beneficial influence of medium basic sites were described elsewhere [10,27,29]. In the current study, the enhancement of moderate basicity can be attributed to the increase of Ce^{3+} ratio shown in XPS. The incorporation of Y resulted in an increase of Ce^{3+} ratio, thus more CO_2 species were adsorbed on the generated oxygen vacancies [10]. However, the total basic sites of catalysts were not satisfactory, which demonstrated the importance of basicity to improve the catalytic performance.

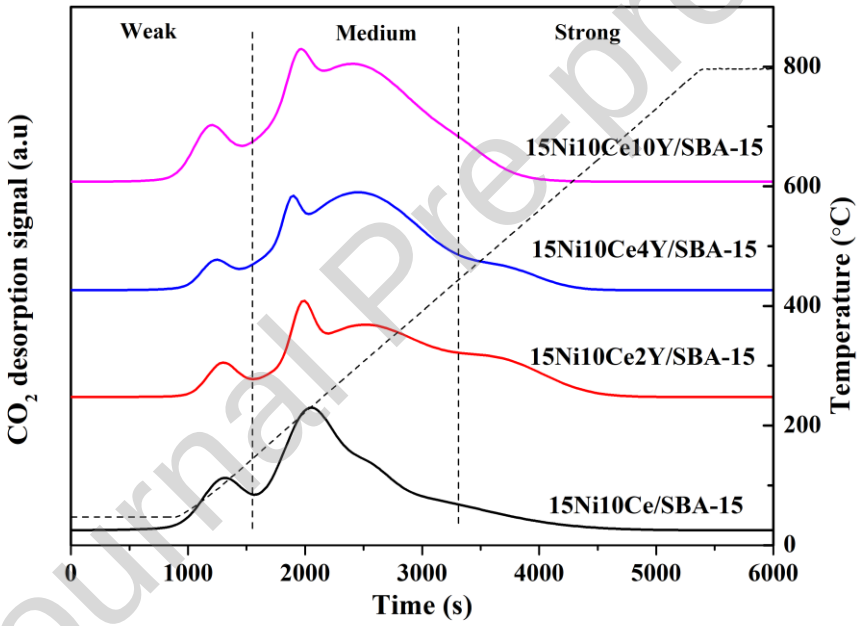

Figure. 6. CO_2 desorption curves of the catalysts after reduction at 550 °C for 1.5h.

Table 3. The basic sites distribution calculated from CO_2-TPD for the reduced catalysts.

Catalyst	Basic sites [μmol/g_{cat}]			Total basic sites [μmol/g_{cat}]	Distribution of basic sites [%]		
	weak	medium	strong		weak	medium	strong
15Ni10Ce/SBA-15	6.7	23.0	8.5	38.2	17.5	60.2	22.3
15Ni10Ce2Y/SBA-15	3.2	38.5	12.4	54.1	5.9	71.2	22.9
15Ni10Ce4Y/SBA-15	2.2	50.5	12.0	64.7	3.4	78.1	18.5
15Ni10Ce10Y/SBA-15	5.4	64.4	11.0	80.8	6.7	79.7	13.6

3.2. Catalytic performance in CO_2 methanation.

The catalytic performance of catalysts in CO_2 methanation was investigated at the temperature range of 200-450 ^oC. In order to confirm the most appropriate loading content of Y, the results of a catalyst with higher Y loading (15%) were also added. The results were displayed in **Fig.7**.

The catalytic activity of NiCe/SBA-15 catalysts promoted with Y is presented in **Fig.7a**. The dashed line represents the thermodynamic equilibrium of CO_2 methanation for the assumed experimental conditions. The CO_2 conversion rate, obtained for the studied catalysts, increased with the increasing reaction temperature and reached nearly equilibrium at 450 °C. In the temperature range of 300-350 °C, in which the conversion values of the catalysts are distinguished, it can be seen that Y promoted catalysts showed higher CO_2 conversion compared to that of 15Ni10Ce/SBA-15. Depending on the loading of yttrium, the following activity order was observed at 350°C: 10Ce (40.0%) < 2Y (44.0%) <15Y (51.1%) < 4Y (54.5%) < 10Y (61.2%), in which 10Ce refers to the

15Ni10Ce/SBA-15 sample. It can be seen that higher Y loading (15wt.% of Y) led to the decrease of CO_2 conversion at 350°C, which indicates that 10wt.% of Y seems to an appropriate content for NiCeY/SBA-15 catalysts.

Fig.7b shows selectivity to CH_4, revealing a gradual decrease with the temperature rise. At the temperatures lower that 300 °C, there is no difference in the CH_4 selectivity for all catalysts as the CO_2 conversion is negligible in this temperature region. In the temperature window between 300 and 400 °C, the Y-free catalyst showed the lowest CH_4 selectivity. Meanwhile, the series of Y-promoted catalysts showed equally high CH_4 selectivity. It is worth noting that only carbon monoxide (CO) was registered as side product in the studied reaction conditions. The formation of CO is mainly caused by the reverse water-gas shift reaction ($CO_2 + H_2 = CO + H_2O$) [83]. According to the thermodynamics of CO_2 methanation reaction, the CO selectivity increases with increasing temperature, consequently decreasing selectivity towards CH_4 production [83,84]. It has been reported that Ce promotion of Ni/SBA-15 catalyst can increase the activity and CH_4 selectivity in CO_2 methanation [31,39]. The presence of cerium can enhance the activation of CO_2 at low temperature, hence improve the activity and CH_4 selectivity [30]. Herein, the promotive effect of Y on NiCe/SBA-15 catalysts was observed.

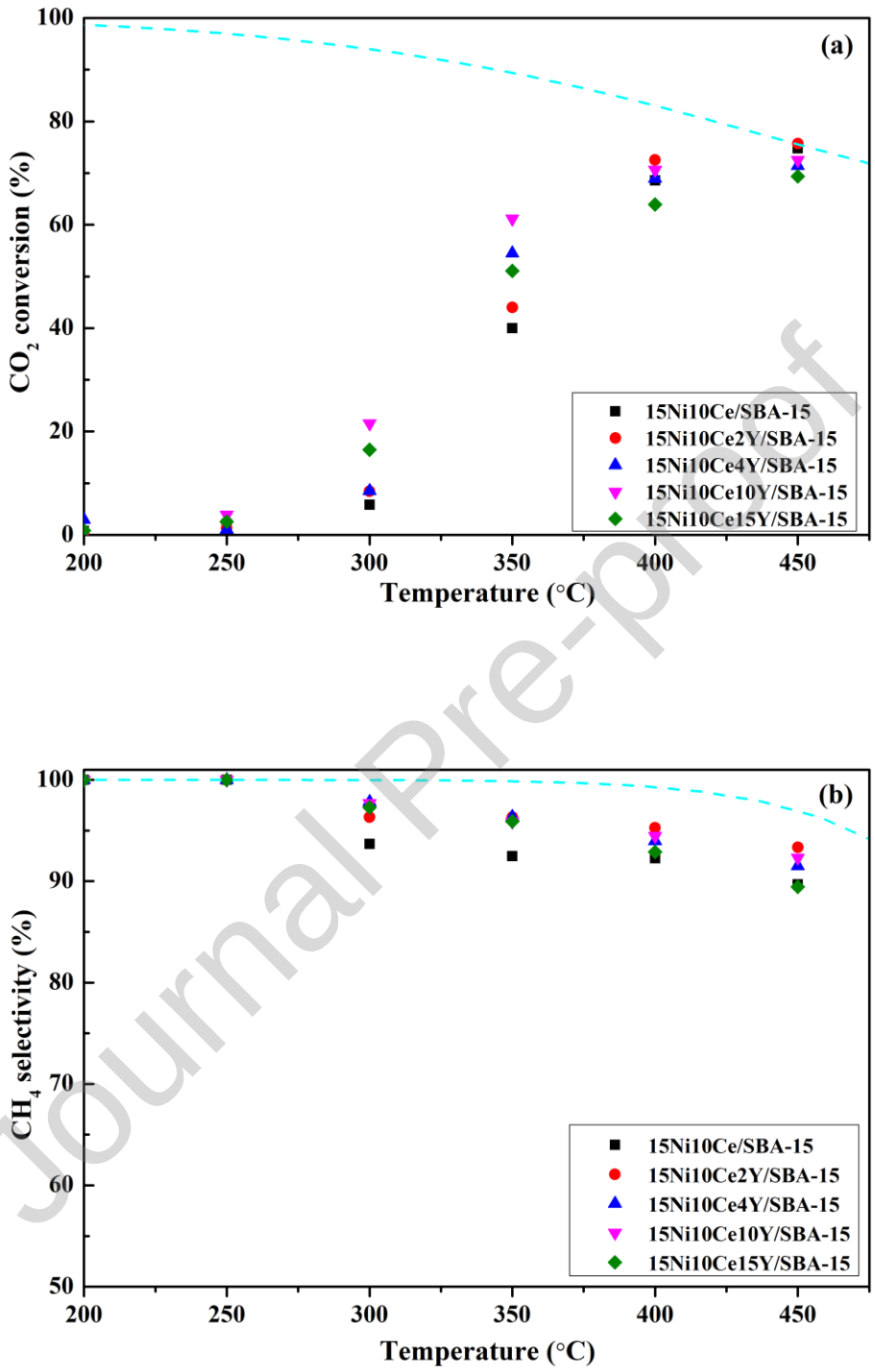

Fig. 7. The catalytic activity in CO_2 methanation of 15Ni10Ce/SBA-15 catalysts with and without yttrium. (a) CO_2 conversion versus temperature; (b) CH_4 selectivity versus temperature. The dotted line represents equilibrium.

It has been reported that the methanation mechanism over Ni-containing SBA-15 and MCM-41 mesoporous silicas undergoes the route of CO free and without participation of intermediates, such as carbonate and formate [30]. In the study of Bacariza et al. [30], FTIR analysis carried out for Ni/SBA-15 catalyst showed that the CO_2 species adsorbed on the surface of Ni metal transformed to carbonate species, following the formation of formate species, then led to the formation of methane. However, many carbonyl species could be formed over the catalysts, which accounted for the formation of CO and the feasible poisoning of metallic Ni. In the CO_2 adsorption experiment carried out with the assistance of FTIR, only CO species (probably originating from the CO_2 disproportionation/dissociation reaction) were found over the bare SBA-15 support, which suggests that the methanation reaction could not occur in the presence of Ni metal [30]. When Ce was loaded onto the Ni/SBA-15 catalyst, the carbonyl species that led to the formation of CO decreased, consequently promoted the activation of CO_2, and enhanced the formation of CH_4. The promotion effect of Ce for Ni/SBA-15 catalyst in CO_2 methanation was undisputed [39]. Moreover, the promoting effect of Y on Ni/CeO_2 catalysts has been reported in CO_2 methanation, in which the addition of Y can lead to an increase of weak and medium basicity, more oxygen vacancies, and enhanced metal-support interaction [10].

In the current study, the presence of Y promoted the reduction of Ni species of 15Ni10CexY/SBA-15 catalysts, as proven by H_2-TPR experiment. Meanwhile, the formation of solid solution of Y-Ce was demonstrated by XPS. Also, the addition of Y could lead to the increased ratio of $Ce^{3+}/(Ce^{3+}+Ce^{4+})$, with 10 wt.% Y-modified catalysts having the highest ratio of $Ce^{3+}/(Ce^{3+}+Ce^{4+})$, and favoring an increase of oxygen

vacancies. The latter is believed to promote the activation CO_2 [10]. Moreover, CO_2-TPD results shows that the presence of yttrium oxide can contribute to the increase of medium-strength basic sites, which are advantageous in CO_2 methanation [82]. In our study, the 10 wt.% Y-modified catalyst presented the highest number of medium basic sites, which can explain the increased CO_2 conversion and CH_4 selectivity.

In **Table S3**, the catalytic activity regarding CH_4 formation rate (r_{CH4}) of NiCeY/SBA-15 catalysts was calculated and compared with those reported catalysts in CO_2 methanation. It can be seen that the catalytic performance of NiCeY/SBA-15 is comparable relative to other catalysts. Although there is still room for improvement of the NiCeY/SBA-15 catalyst, it appears to be a promising candidate for CO_2 methanation.

In order to correlate the catalytic performance of catalysts with the physicochemical properties, the CO_2 reaction rate (r_{CO2}) at 350 ℃ was calculated and correlated with the ratio of $Ce^{3+}/(Ce^{3+}+Ce^{4+})$ and medium basic sites. As shown in **Fig. 8a**, a linear correlation can be found between $Ce^{3+}/(Ce^{3+}+Ce^{4+})$ ratio and Y loading. With increasing Y loading up to 10 wt.%, the ratio of $Ce^{3+}/(Ce^{3+}+Ce^{4+})$ and CO_2 reaction rate increase linearly. Furthermore, CO_2 reaction rate can also be correlated with the amount of medium basic sites, as shown in **Fig. 8b**. A linear correlation between CO_2 reaction rate over catalyst and number of medium basic sites were drawn. Promotion of 15Ni10Ce/SBA-15 catalysts with the appropriate loading of yttrium can improve the Ni dispersion and its reducibility, increase the ratio of $Ce^{3+}/(Ce^{3+}+Ce^{4+})$, and enhance the moderate basicity. All these factors can positively influence catalytic activity in CO_2 methanation reaction.

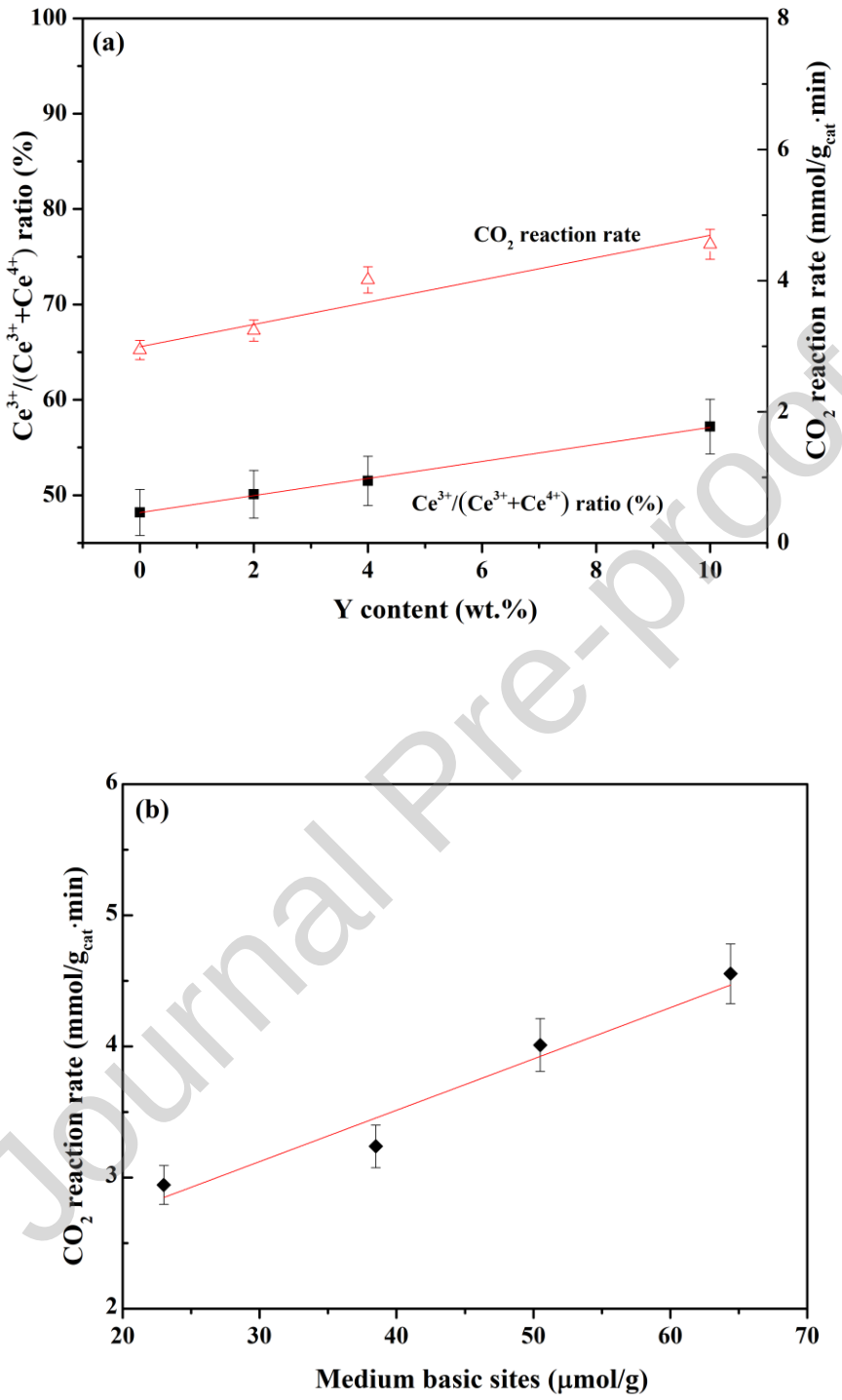

Figure. 8. Correlation between the CO_2 reaction rate at 350 °C and the ratio of $Ce^{3+}/(Ce^{3+}+ Ce^{4+})$ (a) or medium basic sites (b) with the 0 wt.% Y representing the NiCe/SBA-15 sample.

3.3. Stability tests of NiCe/SBA-15 and NiCeY/SBA-15 catalysts at 350 °C

The stability tests were performed at 350°C for 15Ni10Ce/SBA-15, 15Ni10Ce4Y/SBA-15, and 15Ni10Ce10Y/SBA-15 catalysts. **Fig. 9a** shows stable CO_2 conversion values during 7 h of time-on-stream (TOS) experiments. The highest CO_2 conversion was measured for 15Ni10Ce10Y/SBA-15, in good agreement with previously conducted experiments (**Fig. 7b**). In **Fig. 9b**, the catalysts modified with 4 and 10 wt.% of Y showed nearly the same CH_4 selectivity values during the stability test. Nevertheless, the 15Ni10Ce/SBA-15 catalyst showed a slight loss in CH_4 selectivity after 2h test, which may be caused by the formation of Ni carbonyls, leading to the possible sintering of Ni metal and formation of CO species [30]. Carbon monoxide is a side product of parallelly occurring reactions during CO_2 hydrogenation, i.e. reverse-water gas shift [85]. On the other hand, the carbon monoxide production can be associated with a deactivation of metallic nickel nanoparticles. Zurrer et al. [86] studied differently modified NiMg-MOF-74 mixed metals catalysts in CO_2 methanation. The authors reported that the selectivity tends towards CO production rather than CH_4 for the catalysts containing the most content of nickel (80Ni20Mg and 100Ni). Once the nickel particles are encapsulated by graphitic carbon, a reduction of the adsorbed CO intermediate is diminished due to a hydrogen deficient environment. Another explanation can be a change in the nickel metal electronic state caused by the carbon shell formation. In the latter case the resulting product can be carbon monoxide. Both hypotheses imply the importance of usage a carbon-resistant catalyst in CO_2 methanation.

A TOS test more than 24 h for 15Ni10Ce10Y/SBA-15 catalyst was also carried out and displayed in **Fig.S4**. As shown in **Fig.S4**, both the CO_2 conversion and CH_4 selectivity of the catalyst are highly stable during the TOS process, which indicates that there was no significant deactivation during CO_2 methanation process.

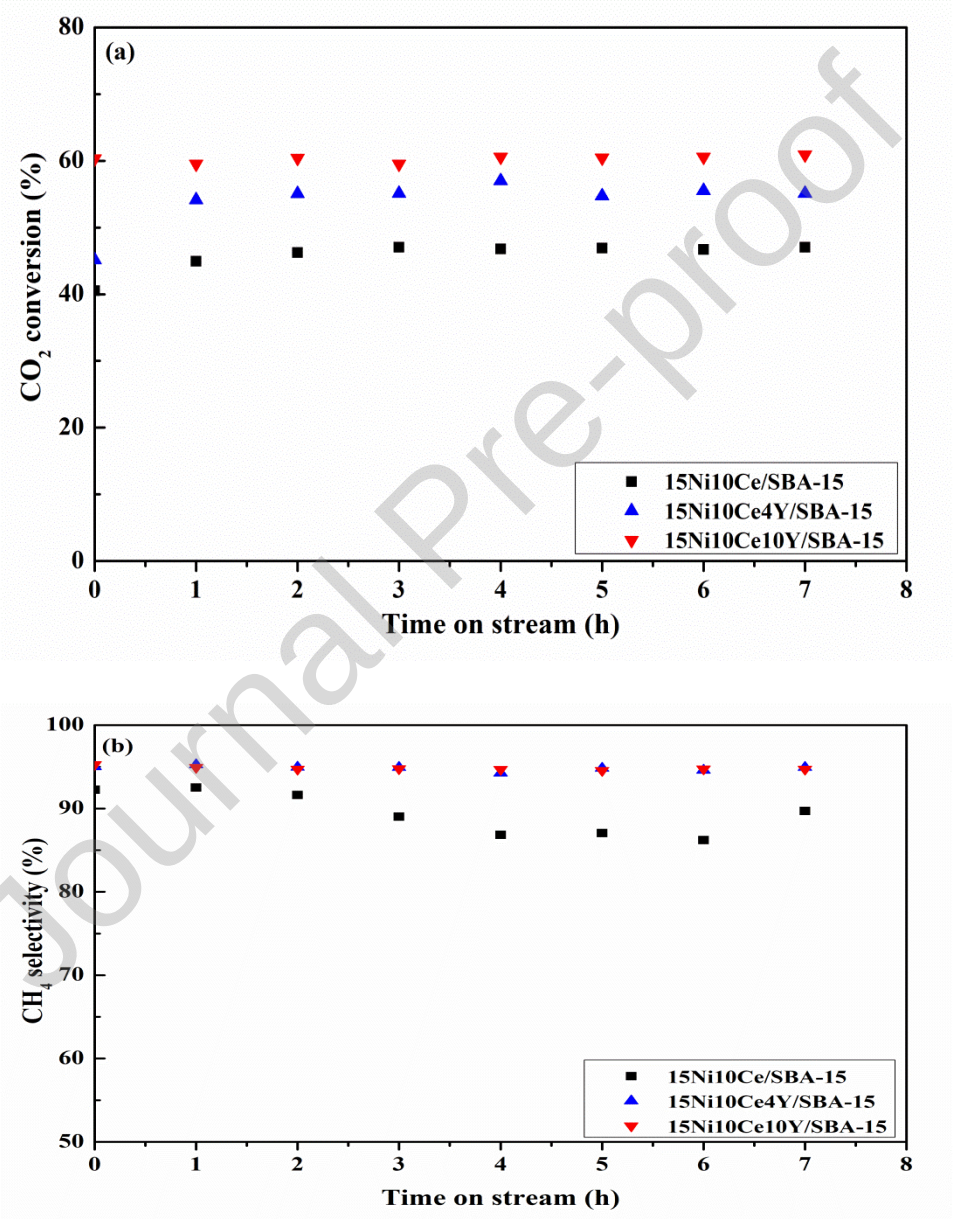

Figure. 9. The stability tests of CO_2 methanation over selected NiCe/SBA-15 and NiCeY/SBA-15 catalysts; (a) CO_2 conversion versus time; (b) CH_4 selectivity versus time. Experimental conditions: 350 °C, $H_2/CO_2/Ar$=60/15/25, GHSV=12,000 h^{-1}.

3.4. Characterization of catalysts after CO_2 methanation reaction.

Wide-angle XRD measurements were carried out to investigate the structural features of the catalysts after CO_2 methanation. **Fig.S5** presents that nearly no changes of the diffraction peaks were registered, compared to the XRD results recorded for the reduced catalysts (**Fig.3b**). This indicates that there is no sintering of nickel during the reaction [29].No reflection peak arising from graphitic carbon was observed. Nevertheless, the crystal size of metallic Ni metal shows neglect change compared with reduced catalysts **(Table S4)**, which may account for the high stability of catalysts.

Thermogravimetric analysis was performed to examine an existence of carbon deposit formed during CO_2 methanation. The registered curves are shown in **Fig. S6**. Spent 15Ni10Ce10Y/SBA-15 catalyst was decomposed in air, revealing formation of products with mass signals of m/z= 18 (H_2O) and m/z= 44 (CO_2). The first weight loss registered in the temperature range from 35 to 200°C can be attributed to the removal of water molecules from SBA-15 supported catalyst. The second mass change occurred between 200 and 400°C and can be related to desorption of the adsorbed molecules during the reaction, e.g. CO_2 (m/z = 44). The mass gain is a result of Ni° oxidation into NiO crystallites [87]. The third mass change was recorded between ca. 400 and 900°C which can be linked with possible oxidation of deposited carbon, however, that was not the case for our spent catalyst as no change of the m/z=44 signal was registered ($C+O_2=CO_2$). Moreover, no mass difference was recorded above 800°C, excluding the existence of graphitic carbon.

Conclusions

The effect of yttrium promotion on SBA-15-supported Ni-Ce catalysts was investigated in this study. A series of NiCeY/SBA-15 catalysts were characterized and tested in CO_2 methanation. The microscopy analyses revealed that modification with Y positively affects the distribution of Ni particles, being extensively dispersed inside the mesoporous channels of SBA-15 silica support. Moreover, yttrium as a promoter contributed to an increase of $Ce^{3+}/(Ce^{3+}+Ce^{4+})$ ratio and number of medium basic sites, enhanced the reducibility of Ni species, and led to the formation of a Y-Ce solid solution. NiCeY/SBA-15 catalysts showed better catalytic performance in CO_2 methanation than Y-free catalyst, with the highest CO_2 conversion and CH_4 selectivity measured for the 10 wt.% Y loading. Both catalysts 15Ni10Ce/SBA-15 and 15Ni10Ce10Y/SBA-15 revealed stable CO_2 conversion without activity loss during a 7 h of time-on-stream (TOS) experiment at 350°C. In addition, the modification with Y favors selective CO_2 hydrogenation towards CH_4 production. 15Ni10Ce10Y/SBA-15 showed excellent coking resistance and anti-sintering ability, which can be attributed to the confinement of SBA-15 structure.

Acknowledgments

Chao Sun would like to express his gratitude to the China Scholarship Council (CSC) for the financial support during his doctoral studies at Sorbonne Universitė. Katarzyna Świrk is an MSCA-IF-funded researcher at Norwegian University of Science and Technology in Trondheim. This project has received funding from the European Union's Horizon 2020 research and innovation programme under the Marie Skłodowska-Curie grant agreement

no. 892571. KSS and DWB thank the Norwegian Research Council for funding through the FRINATEK program (grant 275182) and its Centres of Excellence funding scheme, project number 262644."

References

[1] P. Nema, S. Nema, P. Roy, An overview of global climate changing in current scenario and mitigation action, Renew. Sustain. Energy Rev. 16 (2012) 2329–2336. https://doi.org/10.1016/j.rser.2012.01.044.

[2] M.A.A. Aziz, A.A. Jalil, S. Triwahyono, A. Ahmad, CO2 methanation over heterogeneous catalysts: Recent progress and future prospects, Green Chem. 17 (2015) 2647–2663. https://doi.org/10.1039/c5gc00119f.

[3] C. Song, Global challenges and strategies for control, conversion and utilization of CO2 for sustainable development involving energy, catalysis, adsorption and chemical processing, Catal. Today. 115 (2006) 2–32. https://doi.org/10.1016/j.cattod.2006.02.029.

[4] E.S. Rubin, J.E. Davison, H.J. Herzog, The cost of CO2 capture and storage, Int. J. Greenh. Gas Control. 40 (2015) 378–400. https://doi.org/10.1016/j.ijggc.2015.05.018.

[5] K.M.K. Yu, I. Curcic, J. Gabriel, S.C.E. Tsang, Recent advances in CO2 capture and utilization., ChemSusChem. 1 (2008) 893–899. https://doi.org/10.1002/cssc.200800169.

[6] Y. Wang, Q. Zhao, Y. Wang, C. Hu, P. Da Costa, One-Step Synthesis of Highly Active and Stable Ni-ZrOx for Dry Reforming of Methane, Ind. Eng. Chem. Res.

59 (2020) 11441–11452. https://doi.org/10.1021/acs.iecr.0c01416.

[7] Y. Wang, L. Li, Y. Wang, P. Da Costa, C. Hu, Highly carbon-resistant Y doped NiO–ZrOm catalysts for dry reforming of methane, Catalysts. 9 (2019) 1055. https://doi.org/10.3390/catal9121055.

[8] Y. Wang, L. Yao, Y. Wang, S. Wang, Q. Zhao, D. Mao, C. Hu, Low-Temperature Catalytic CO2 Dry Reforming of Methane on Ni-Si/ZrO2 Catalyst, ACS Catal. 8 (2018) 6495–6506. https://doi.org/10.1021/acscatal.8b00584.

[9] C. Sun, K. Świrk, D. Wierzbicki, M. Motak, T. Grzybek, P. Da Costa, On the effect of yttrium promotion on Ni-layered double hydroxides-derived catalysts for hydrogenation of CO2 to methane, Int. J. Hydrogen Energy. 46 (2021) 12169–12179. https://doi.org/10.1016/j.ijhydene.2020.03.202.

[10] C. Sun, P. Beaunier, V. La Parola, L. F. Liotta, P. Da Costa, Ni/CeO2 Nanoparticles Promoted by Yttrium Doping as Catalysts for CO2 Methanation, ACS Appl. Nano Mater. 3 (2020) 12355–12368. https://doi.org/10.1021/acsanm.0c02841.

[11] C. Sun, P. Beaunier, P. Da Costa, Effect of ceria promotion on the catalytic performance of Ni/SBA-16 catalysts for CO2 methanation, Catal. Sci. Technol. 10 (2020) 6330–6341. https://doi.org/10.1039/d0cy00922a.

[12] W.H. Wang, Y. Himeda, J.T. Muckerman, G.F. Manbeck, E. Fujita, CO2 Hydrogenation to Formate and Methanol as an Alternative to Photo- and Electrochemical CO2 Reduction, Chem. Rev. 115 (2015) 12936–12973. https://doi.org/10.1021/acs.chemrev.5b00197.

[13] B. Liu, B. Ouyang, Y. Zhang, K. Lv, Q. Li, Y. Ding, J. Li, Effects of mesoporous

structure and Pt promoter on the activity of Co-based catalysts in low-temperature CO2 hydrogenation for higher alcohol synthesis, J. Catal. 366 (2018) 91–97. https://doi.org/10.1016/j.jcat.2018.07.019.

[14] A. Álvarez, A. Bansode, A. Urakawa, A. V. Bavykina, T.A. Wezendonk, M. Makkee, J. Gascon, F. Kapteijn, Challenges in the Greener Production of Formates/Formic Acid, Methanol, and DME by Heterogeneously Catalyzed CO2 Hydrogenation Processes, Chem. Rev. 117 (2017) 9804–9838. https://doi.org/10.1021/acs.chemrev.6b00816.

[15] G. Zhou, H. Liu, K. Cui, H. Xie, Z. Jiao, G. Zhang, K. Xiong, X. Zheng, Methanation of carbon dioxide over Ni/CeO2 catalysts: Effects of support CeO2 structure, Int. J. Hydrogen Energy. 42 (2017) 16108–16117. https://doi.org/10.1016/j.ijhydene.2017.05.154.

[16] P.A. Ussa Aldana, F. Ocampo, K. Kobl, B. Louis, F. Thibault-Starzyk, M. Daturi, P. Bazin, S. Thomas, A.C.C. Roger, P.A.U. Aldana, F. Ocampo, K. Kobl, B. Louis, F. Thibault-Starzyk, M. Daturi, P. Bazin, S. Thomas, A.C.C. Roger, Catalytic CO2 valorization into CH4 on Ni-based ceria-zirconia. Reaction mechanism by operando IR spectroscopy, Catal. Today. 215 (2013) 201–207. https://doi.org/10.1016/j.cattod.2013.02.019.

[17] H. Liu, S. Xu, G. Zhou, K. Xiong, Z. Jiao, S. Wang, CO2 hydrogenation to methane over Co/KIT-6 catalysts: Effect of Co content, Fuel. 217 (2018) 570–576. https://doi.org/10.1016/j.fuel.2017.12.112.

[18] J.N. Park, E.W. McFarland, A highly dispersed Pd-Mg/SiO2 catalyst active for methanation of CO2, J. Catal. 266 (2009) 92–97.

https://doi.org/10.1016/j.jcat.2009.05.018.

[19] A. Karelovic, P. Ruiz, Mechanistic study of low temperature CO2 methanation over Rh/TiO2 catalysts, J. Catal. 301 (2013) 141–153. https://doi.org/10.1016/j.jcat.2013.02.009.

[20] R.P. Ye, Q. Li, W. Gong, T. Wang, J.J. Razink, L. Lin, Y.Y. Qin, Z. Zhou, H. Adidharma, J. Tang, A.G. Russell, M. Fan, Y.G. Yao, High-performance of nanostructured Ni/CeO2 catalyst on CO2 methanation, Appl. Catal. B Environ. 268 (2019) 118474. https://doi.org/10.1016/j.apcatb.2019.118474.

[21] S. Tada, T. Shimizu, H. Kameyama, T. Haneda, R. Kikuchi, Ni/CeO2 catalysts with high CO2 methanation activity and high CH4 selectivity at low temperatures, Int. J. Hydrogen Energy. 37 (2012) 5527–5531. https://doi.org/10.1016/j.ijhydene.2011.12.122.

[22] C. Liang, X. Hu, T. Wei, P. Jia, Z. Zhang, Methanation of CO2 over Ni/Al2O3 modified with alkaline earth metals : Impacts of oxygen vacancies on catalytic activity, Int. J. Hydrogen Energy. 44 (2019) 8197–8213. https://doi.org/10.1016/j.ijhydene.2019.02.014.

[23] M. Younas, L. Loong Kong, M.J.K. Bashir, H. Nadeem, A. Shehzad, S. Sethupathi, Recent Advancements, Fundamental Challenges, and Opportunities in Catalytic Methanation of CO2, Energy and Fuels. 30 (2016) 8815–8831. https://doi.org/10.1021/acs.energyfuels.6b01723.

[24] M. Li, H. Amari, A.C. van Veen, Metal-oxide interaction enhanced CO2 activation in methanation over ceria supported nickel nanocrystallites, Appl. Catal. B Environ. 239 (2018) 27–35. https://doi.org/10.1016/j.apcatb.2018.07.074.

[25] M. Romero-Sáez, A.B. Dongil, N. Benito, R. Espinoza-González, N. Escalona, F. Gracia, CO2 methanation over nickel-ZrO2 catalyst supported on carbon nanotubes: A comparison between two impregnation strategies, Appl. Catal. B Environ. 237 (2018) 817–825. https://doi.org/10.1016/j.apcatb.2018.06.045.

[26] Garbarino Gabriella, Riani Paola, M. Loredana, Busca Guido, A study of the methanation of carbon dioxide on Ni/Al2O3 catalysts at atmospheric pressure, Int. J. Hydrogen Energy. 39 (2014) 11557–11565. https://doi.org/http://dx.doi.org/10.1016/j.ijhydene.2014.05.111.

[27] K. Świrk, P. Summa, D. Wierzbicki, M. Motak, P. Da Costa, Vanadium promoted Ni(Mg,Al)O hydrotalcite-derived catalysts for CO2 methanation, Int. J. Hydrogen Energy. (2021). https://doi.org/https://doi.org/10.1016/j.ijhydene.2021.02.172.

[28] H.C. Wu, Y.C. Chang, J.H. Wu, J.H. Lin, I.K. Lin, C.S. Chen, Methanation of CO2 and reverse water gas shift reactions on Ni/SiO2 catalysts: the influence of particle size on selectivity and reaction pathway, Catal. Sci. Technol. 5 (2015) 4154–4163. https://doi.org/10.1039/C5CY00667H.

[29] P. Hongmanorom, J. Ashok, G. Zhang, Z. Bian, M.H. Wai, Y. Zeng, S. Xi, A. Borgna, S. Kawi, Enhanced performance and selectivity of CO2 methanation over phyllosilicate structure derived Ni-Mg/SBA-15 catalysts, Appl. Catal. B Environ. 282 (2021) 119564. https://doi.org/10.1016/j.apcatb.2020.119564.

[30] M.C. Bacariza, I. Graça, S.S. Bebiano, J.M. Lopes, C. Henriques, Micro- and mesoporous supports for CO2 methanation catalysts: A comparison between SBA-15, MCM-41 and USY zeolite, Chem. Eng. Sci. 175 (2018) 72–83. https://doi.org/10.1016/j.ces.2017.09.027.

[31] L. Wang, H. Liu, H. Ye, R. Hu, S. Yang, G. Tang, K. Li, Y. Yang, Vacuum thermal treated Ni-CeO2/SBA-15 catalyst for CO2 methanation, Nanomaterials. 8 (2018) 1–10. https://doi.org/10.3390/nano8100759.

[32] Q. Liu, Y. Tian, One-pot synthesis of NiO/SBA-15 monolith catalyst with a three-dimensional framework for CO2 methanation, Int. J. Hydrogen Energy. 42 (2017) 12295–12300. https://doi.org/10.1016/j.ijhydene.2017.02.070.

[33] X. Wang, L. Zhu, Y. Liu, S. Wang, CO2 methanation on the catalyst of Ni/MCM-41 promoted with CeO2, Sci. Total Environ. 625 (2018) 686–695. https://doi.org/10.1016/j.scitotenv.2017.12.308.

[34] G. Du, S. Lim, Y. Yang, C. Wang, L. Pfefferle, G.L. Haller, Methanation of carbon dioxide on Ni-incorporated MCM-41 catalysts: The influence of catalyst pretreatment and study of steady-state reaction, J. Catal. 249 (2007) 370–379. https://doi.org/10.1016/j.jcat.2007.03.029.

[35] K. Świrk, M.E. Gálvez, M. Motak, T. Grzybek, M. Rønning, P. Da Costa, Syngas production from dry methane reforming over yttrium-promoted nickel-KIT-6 catalysts, Int. J. Hydrogen Energy. 44 (2019) 274–286. https://doi.org/10.1016/j.ijhydene.2018.02.164.

[36] C.S. Budi, H.C. Wu, C.S. Chen, D. Saikia, H.M. Kao, Ni Nanoparticles Supported on Cage-Type Mesoporous Silica for CO2 Hydrogenation with High CH4 Selectivity, ChemSusChem. 9 (2016) 2326–2331. https://doi.org/10.1002/cssc.201600710.

[37] E.A.C. Panduro, H. Granlund, M. Sztucki, O. Konovalov, D.W. Breiby, A. Gibaud, Using three-dimensional 3D grazing-incidence small-angle X-ray

scattering (GISAXS) analysis to probe pore deformation in mesoporous silica films, ACS Appl. Mater. Interfaces. 6 (2014) 2686–2691. https://doi.org/10.1021/am404602t.

[38] B. Li, S. Zhang, Methane reforming with CO2 using nickel catalysts supported on yttria-doped SBA-15 mesoporous materials via sol-gel process, Int. J. Hydrogen Energy. 38 (2013) 14250–14260. https://doi.org/10.1016/j.ijhydene.2013.08.105.

[39] L. Bian, L. Zhang, Z. Zhu, Z. Li, Methanation of carbon oxides on Ni/Ce/SBA-15 pretreated with dielectric barrier discharge plasma, Mol. Catal. 446 (2018) 131–139. https://doi.org/10.1016/j.mcat.2017.12.027.

[40] H. Li, J. Ren, X. Qin, Z. Qin, J. Lin, Z. Li, Ni/SBA-15 catalysts for CO methanation: effects of V, Ce, and Zr promoters, RSC Adv. 5 (2015) 96504–96517. https://doi.org/10.1039/c5ra15990c.

[41] N. Abdullah, N. Ainirazali, H. Ellapan, Structural effect of Ni/SBA-15 by Zr promoter for H2 production via methane dry reforming, Int. J. Hydrogen Energy. (2020). https://doi.org/10.1016/j.ijhydene.2020.07.060.

[42] H. Wan, X. Li, S. Ji, B. Huang, K. Wang, C. Li, Effect of Ni Loading and CexZri-xO2 Promoter on Ni-Based SBA-15 Catalysts for Steam Reforming of Methane, J. Nat. Gas Chem. 16 (2007) 139–147. https://doi.org/10.1016/S1003-9953(07)60039-5.

[43] J.F. Li, C. Xia, C.T. Au, B.S. Liu, Y2O3-promoted NiO/SBA-15 catalysts highly active for CO2/CH4 reforming, Int. J. Hydrogen Energy. 39 (2014) 10927–10940. https://doi.org/10.1016/j.ijhydene.2014.05.021.

[44] C.C. Chong, L.P. Teh, H.D. Setiabudi, Syngas production via CO2 reforming of

CH4 over Ni-based SBA-15: Promotional effect of promoters (Ce, Mg, and Zr), Mater. Today Energy. 12 (2019) 408–417. https://doi.org/10.1016/j.mtener.2019.04.001.

[45] C. Liu, J. Zhou, H. Ma, W. Qian, H. Zhang, W. Ying, Antisintering and High-Activity Ni Catalyst Supported on Mesoporous Silica Incorporated by Ce/Zr for CO Methanation, Ind. Eng. Chem. Res. 57 (2018) 14406–14416. https://doi.org/10.1021/acs.iecr.8b03254.

[46] A. Albarazi, P. Beaunier, P. Da Costa, Hydrogen and syngas production by methane dry reforming on SBA-15 supported nickel catalysts: On the effect of promotion by Ce0.75Zr 0.25O2 mixed oxide, Int. J. Hydrogen Energy. 38 (2013) 127–139. https://doi.org/10.1016/j.ijhydene.2012.10.063.

[47] X. Wang, L. Zhu, Y. Zhuo, Y. Zhu, S. Wang, Enhancement of CO2 Methanation over La-Modified Ni/SBA-15 Catalysts Prepared by Different Doping Methods, ACS Sustain. Chem. Eng. 7 (2019) 14647–14660. https://doi.org/10.1021/acssuschemeng.9b02563.

[48] Y.F. Han, F. Chen, Z. Zhong, K. Ramesh, L. Chen, E. Widjaja, Controlled synthesis, characterization, and catalytic properties of Mn2O3 and Mn3O4 nanoparticles supported on mesoporous silica SBA-15, J. Phys. Chem. B. 110 (2006) 24450–24456. https://doi.org/10.1021/jp064941v.

[49] R.K. Singha, A. Shukla, A. Yadav, L.N. Sivakumar Konathala, R. Bal, Effect of metal-support interaction on activity and stability of Ni-CeO2 catalyst for partial oxidation of methane, Appl. Catal. B Environ. 202 (2017) 473–488. https://doi.org/10.1016/j.apcatb.2016.09.060.

[50] C.C. Chong, A.H.K. Owgi, N. Ainirazali, S.Y. Chin, H.D. Setiabudi, CO2 reforming of CH4 over Ni/SBA-15 prepared by surfactant-assisted impregnation method: Comparative study of surfactant types, Mater. Today Proc. 5 (2018) 21644–21651. https://doi.org/10.1016/j.matpr.2018.07.014.

[51] M.A. Naeem, A.S. Al-Fatesh, A.H. Fakeeha, A.E. Abasaeed, Hydrogen production from methane dry reforming over nickel-based nanocatalysts using surfactant-assisted or polyol method, Int. J. Hydrogen Energy. 39 (2014) 17009–17023. https://doi.org/10.1016/j.ijhydene.2014.08.090.

[52] J. Filik, A.W. Ashton, P.C.Y. Chang, P.A. Chater, S.J. Day, M. Drakopoulos, M.W. Gerring, M.L. Hart, O. V. Magdysyuk, S. Michalik, A. Smith, C.C. Tang, N.J. Terrill, M.T. Wharmby, H. Wilhelm, Processing two-dimensional X-ray diffraction and small-angle scattering data in DAWN 2, J. Appl. Crystallogr. 50 (2017) 959–966. https://doi.org/10.1107/S1600576717004708.

[53] D.W. Breiby, O. Bunk, J.W. Andreasen, H.T. Lemke, M.M. Nielsen, Simulating X-ray diffraction of textured films, J. Appl. Crystallogr. 41 (2008) 262–271. https://doi.org/10.1107/S0021889808001064.

[54] G. Varvoutis, M. Lykaki, S. Stefa, V. Binas, G.E. Marnellos, M. Konsolakis, Deciphering the role of Ni particle size and nickel-ceria interfacial perimeter in the low-temperature CO2 methanation reaction over remarkably active Ni/CeO2 nanorods, Appl. Catal. B Environ. 297 (2021) 120401. https://doi.org/10.1016/j.apcatb.2021.120401.

[55] Y. Kathiraser, J. Ashok, S. Kawi, Synthesis and evaluation of highly dispersed SBA-15 supported Ni-Fe bimetallic catalysts for steam reforming of biomass

derived tar reaction, Catal. Sci. Technol. 6 (2016) 4327–4336. https://doi.org/10.1039/c5cy01910a.

[56] Q. Zhang, M. Wang, T. Zhang, Y. Wang, X. Tang, P. Ning, A stable Ni/SBA-15 catalyst prepared by the ammonia evaporation method for dry reforming of methane, RSC Adv. 5 (2015) 94016–94024. https://doi.org/10.1039/c5ra18845h.

[57] R. Gómez-Reynoso, J. Ramírez, R. Nares, R. Luna, F. Murrieta, Characterization and catalytic activity of Ni/SBA-15, synthesized by deposition-precipitation, Catal. Today. 107–108 (2005) 926–932. https://doi.org/10.1016/j.cattod.2005.07.152.

[58] Z. Taherian, M. Yousefpour, M. Tajally, B. Khoshandam, A comparative study of ZrO2, Y2O3 and Sm2O3 promoted Ni/SBA-15 catalysts for evaluation of CO2/methane reforming performance, Int. J. Hydrogen Energy. 42 (2017) 16408–16420. https://doi.org/10.1016/j.ijhydene.2017.05.095.

[59] A. Ungureanu, B. Dragoi, A. Chirieac, C. Ciotonea, S. Royer, D. Duprez, A.S. Mamede, E. Dumitriu, Composition-Dependent Morphostructural Properties of Ni-Cu Oxide Nanoparticles Confined within the Channels of Ordered Mesoporous SBA-15 Silica, ACS Appl. Mater. Interfaces. 5 (2013) 3010–3025. https://doi.org/10.1021/am302733m.

[60] N. Wang, W. Chu, T. Zhang, X.S. Zhao, Synthesis, characterization and catalytic performances of Ce-SBA-15 supported nickel catalysts for methane dry reforming to hydrogen and syngas, Int. J. Hydrogen Energy. 37 (2012) 19–30. https://doi.org/10.1016/j.ijhydene.2011.03.138.

[61] Q.H. Dongyuan Zhao, Jianglin Feng, G.D.S. Nicholas Melosh, Glenn H. Fredrickson, Bradley F. Chmelka, Triblock Copolymer Syntheses of Mesoporous

Silica with Periodic 50 to 300 Angstrom Pores, Science (80-.). 279 (1998) 548–552. https://doi.org/10.1126/science.279.5350.548.

[62] D. Xia, Y. Chen, C. Li, C. Liu, G. Zhou, Carbon dioxide reforming of methane to syngas over ordered mesoporous Ni/KIT-6 catalysts, Int. J. Hydrogen Energy. 43 (2018) 20488–20499. https://doi.org/10.1016/j.ijhydene.2018.09.059.

[63] U. Oemar, Y. Kathiraser, M.L. Ang, K. Hidajat, S. Kawi, Catalytic Biomass Gasification to Syngas over Highly Dispersed Lanthanum-Doped Nickel on SBA-15, ChemCatChem. 7 (2015) 3376–3385. https://doi.org/10.1002/cctc.201500482.

[64] V. Shanmugam, R. Zapf, S. Neuberg, V. Hessel, G. Kolb, Effect of ceria and zirconia promotors on Ni/SBA-15 catalysts for coking and sintering resistant steam reforming of propylene glycol in microreactors, Appl. Catal. B Environ. 203 (2017) 859–869. https://doi.org/10.1016/j.apcatb.2016.10.075.

[65] K. Świrk, M. Rønning, M. Motak, P. Beaunier, P. Da Costa, T. Grzybek, Ce- and Y-Modified Double-Layered Hydroxides as Catalysts for Dry Reforming of Methane: On the Effect of Yttrium Promotion, Catalysts. 9 (2019) 56. https://doi.org/10.3390/catal9010056.

[66] G. Pantaleo, V. La Parola, F. Deganello, R.K. Singha, R. Bal, A.M. Venezia, Ni/CeO2 catalysts for methane partial oxidation: Synthesis driven structural and catalytic effects, Appl. Catal. B Environ. 189 (2016) 233–241. https://doi.org/10.1016/j.apcatb.2016.02.064.

[67] M. Kang, E.D. Park, J.M. Kim, J.E. Yie, Manganese oxide catalysts for NOx reduction with NH3 at low temperatures, Appl. Catal. A Gen. 327 (2007) 261–269. https://doi.org/10.1016/j.apcata.2007.05.024.

[68] F. Larachi, J. Pierre, A. Adnot, A. Bernis, Ce 3d XPS study of composite Ce x Mn 1-x O 2-y wet oxidation catalysts, Appl. Surf. Sci. 195 (2002) 236–250. https://doi.org/10.1016/S0169-4332(02)00559-7.

[69] G. Munteanu, P. Petrova, I. Ivanov, L.F. Liotta, Z. Kaszkur, T. Tabakova, L. Ilieva, Temperature-programmed reduction of lightly yttrium-doped Au/CeO2 catalysts: Correlation between oxygen mobility and WGS activity, J. Therm. Anal. Calorim. 131 (2018) 145–154. https://doi.org/10.1007/s10973-017-6475-1.

[70] M. Burbano, S.T. Norberg, S. Hull, S.G. Eriksson, D. Marrocchelli, P.A. Madden, G.W. Watson, Oxygen vacancy ordering and the conductivity maximum in Y2O3-Doped CeO2, Chem. Mater. 24 (2012) 222–229. https://doi.org/10.1021/cm2031152.

[71] J. Yang, R. Wang, L. Yang, J. Lang, M. Wei, M. Gao, X. Liu, J. Cao, X. Li, N. Yang, Tunable deep-level emission in ZnO nanoparticles via yttrium doping, J. Alloys Compd. 509 (2011) 3606–3612. https://doi.org/10.1016/j.jallcom.2010.12.102.

[72] J.K. Kesavan, I. Luisetto, S. Tuti, C. Meneghini, G. Iucci, C. Battocchio, S. Mobilio, S. Casciardi, R. Sisto, Nickel supported on YSZ: The effect of Ni particle size on the catalytic activity for CO2 methanation, J. CO2 Util. 23 (2018) 200–211. https://doi.org/10.1016/j.jcou.2017.11.015.

[73] G. Zhou, H. Liu, K. Cui, A. Jia, G. Hu, Z. Jiao, Y. Liu, X. Zhang, Role of surface Ni and Ce species of Ni/CeO2 catalyst in CO2 methanation, Appl. Surf. Sci. 383 (2016) 248–252. https://doi.org/10.1016/j.apsusc.2016.04.180.

[74] X. Jia, X. Zhang, N. Rui, X. Hu, C. jun Liu, Structural effect of Ni/ZrO2 catalyst

on CO2 methanation with enhanced activity, Appl. Catal. B Environ. 244 (2019) 159–169. https://doi.org/10.1016/j.apcatb.2018.11.024.

[75] X. Du, D. Zhang, L. Shi, R. Gao, J. Zhang, Morphology dependence of catalytic properties of Ni/CeO2 nanostructures for carbon dioxide reforming of methane, J. Phys. Chem. C. 116 (2012) 10009–10016. https://doi.org/10.1021/jp300543r.

[76] ‡ and V. Rives‡ J. M. Ferna´ndez,† C. Barriga,† M. A. Ulibarri,*,† F. M. Labajos, New Hydrotalcite-like Compounds Containing Yttrium, Chem Mater. 9 (1997) 312–318.

[77] Y. Guo, J. Zou, X. Shi, P. Rukundo, Z.J. Wang, A Ni/CeO2-CDC-SiC Catalyst with Improved Coke Resistance in CO2 Reforming of Methane, ACS Sustain. Chem. Eng. 5 (2017) 2330–2338. https://doi.org/10.1021/acssuschemeng.6b02661.

[78] H.D. Setiabudi, C.C. Chong, S.M. Abed, L.P. Teh, S.Y. Chin, Comparative study of Ni-Ce loading method: Beneficial effect of ultrasonic-assisted impregnation method in CO2 reforming of CH4 over Ni-Ce/SBA-15, J. Environ. Chem. Eng. 6 (2018) 745–753. https://doi.org/10.1016/j.jece.2018.01.001.

[79] D. Li, L. Zeng, X. Li, X. Wang, H. Ma, S. Assabumrungrat, J. Gong, Ceria-promoted Ni/SBA-15 catalysts for ethanol steam reforming with enhanced activity and resistance to deactivation, Appl. Catal. B Environ. 176–177 (2015) 532–541. https://doi.org/10.1016/j.apcatb.2015.04.020.

[80] S.M. Sidik, S. Triwahyono, A.A. Jalil, M.A.A. Aziz, N.A.A. Fatah, L.P. Teh, Tailoring the properties of electrolyzed Ni/mesostructured silica nanoparticles (MSN) via different Ni-loading methods for CO2 reforming of CH4, J. CO2 Util. 13 (2016) 71–80. https://doi.org/10.1016/j.jcou.2015.12.004.

[81] U. Oemar, Y. Kathiraser, L. Mo, X.K. Ho, S. Kawi, CO2 reforming of methane over highly active La-promoted Ni supported on SBA-15 catalysts: Mechanism and kinetic modelling, Catal. Sci. Technol. 6 (2016) 1173–1186. https://doi.org/10.1039/c5cy00906e.

[82] Q. Pan, J. Peng, T. Sun, S.S. Wang, S.S. Wang, P. Qiushi, J. Peng, T. Sun, S.S. Wang, S.S. Wang, J. Peng, Q. Pan, Insight into the reaction route of CO2 methanation: Promotion effect of medium basic sites, Catal. Commun. 45 (2014) 74–78. https://doi.org/10.1016/j.catcom.2013.10.034.

[83] S. Sahebdelfar, M. Takht Ravanchi, Carbon dioxide utilization for methane production: A thermodynamic analysis, J. Pet. Sci. Eng. 134 (2015) 14–22. https://doi.org/10.1016/j.petrol.2015.07.015.

[84] B. Lu, K. Kawamoto, Direct synthesis of highly loaded and well-dispersed NiO/SBA-15 for producer gas conversion, RSC Adv. 2 (2012) 6800–6805. https://doi.org/10.1039/c2ra20344h.

[85] B. Lu, K. Kawamoto, Preparation of monodispersed NiO particles in SBA-15, and its enhanced selectivity for reverse water gas shift reaction, J. Environ. Chem. Eng. 1 (2013) 300–309. https://doi.org/10.1016/j.jece.2013.05.008.

[86] T. Zurrer, K. Wong, J. Horlyck, E.C. Lovell, J. Wright, N.M. Bedford, Z. Han, K. Liang, J. Scott, R. Amal, Mixed-Metal MOF-74 Templated Catalysts for Efficient Carbon Dioxide Capture and Methanation, Adv. Funct. Mater. 31 (2020) 2007624. https://doi.org/10.1002/adfm.202007624.

[87] Y.R. Dias, O.W. Perez-Lopez, Carbon dioxide methanation over Ni-Cu/SiO2 catalysts, Energy Convers. Manag. 203 (2020) 112214.

https://doi.org/10.1016/j.enconman.2019.112214.

Highlights

- Y promotion of Ni-Ce/SBA-15 catalyst significantly improved the catalytic activity in CO_2 methanation
- 10 wt.% loading of Y showed the highest CO_2 conversion at 350 °C.
- Y promotion led to higher reducibility of nickel species.
- Higher ratio of $Ce^{3+}/(Ce^{3+}+Ce^{4+})$ was found for 10 wt.% Y modified Ni-Ce/SBA-15 catalyst.
- 10 wt.% Y modified Ni-Ce/SBA-15 catalyst showed enhanced stability in CO_2 methanation reaction

Credit author statement CS

Chao Sun, Investigation, Validation, Writing - Original Draft, Review & Editing
Katarzyna Świrk, Investigation, Methodology, Validation, Writing - Original Draft, Review & Editing, Funding acquisition
Ye Wang, Investigation, Validation, Writing - Original Draft, Review & Editing
Katharina Scheidl, Methodology, Validation,
Dag Werner Breiby, Methodology, Validation,
Magnus Rønning, Methodology, Conceptualization,Resources, Writing - Review & Editing, Funding acquisition
Changwei Hu, Methodology, Writing - Review & Editing, Funding acquisition
Patrick Da Costa, Methodology, Supervision, Conceptualization,Resources, Writing - Review & Editing, Funding acquisition

Declaration of interests

☒ The authors declare that they have no known competing financial interests or personal relationships that could have appeared to influence the work reported in this paper.

☐The authors declare the following financial interests/personal relationships which may be considered as potential competing interests: